The functions of SARS-CoV-2 neutralizing and infection-enhancing antibodies in vitro and in mice and nonhuman primates

Dapeng Li[1,2*], Robert J Edwards[1,2*], Kartik Manne[1,2*], David R. Martinez[3,*], Alexandra Schäfer[3,*], S. Munir Alam[1,2], Kevin Wiehe[1,2], Xiaozhi Lu[1,2], Robert Parks[1,2], Laura L. Sutherland[1,2], Thomas H. Oguin III[1,2], Charlene McDanal[4], Lautaro G. Perez[4], Katayoun Mansouri[1,2], Sophie M. C. Gobeil[1,2], Katarzyna Janowska[1,2], Victoria Stalls[1,2], Megan Kopp[1,2], Fangping Cai[1,2], Esther Lee[1,2], Andrew Foulger[1,2], Giovanna E. Hernandez[1,2], Aja Sanzone[1,2], Kedamawit Tilahun[1,2], Chuancang Jiang[1,2], Longping V. Tse[3], Kevin W. Bock[4], Mahnaz Minai[4], Bianca M. Nagata[4], Kenneth Cronin[1,2], Victoria Gee-Lai[1,2], Margaret Deyton[1,2], Maggie Barr[1,2], Tarra Von Holle[1,2], Andrew N. Macintyre[1,2], Erica Stover[1,2], Jared Feldman[6], Blake M. Hauser[6], Timothy M. Caradonna[6], Trevor D. Scobey[3], M. Anthony Moody[1,7], Derek W. Cain[1,2], C. Todd DeMarco[1,2], Thomas N. Denny[1,2], Christopher W. Woods[1,2,8], Elizabeth W. Petzold[8], Aaron G. Schmidt[6,9], I-Ting Teng[10], Tongqing Zhou[10], Peter D. Kwong[10,11], John R. Mascola[10], Barney S. Graham[10], Ian N. Moore[4], Robert Seder[10], Hanne Andersen[12], Mark G. Lewis[12], David C. Montefiori[5], Gregory D. Sempowski[1,2], Ralph S. Baric[3], Priyamvada Acharya[1,5], Barton F. Haynes[1,2,13,#], Kevin O. Saunders[1,5,13,14,#]

[1]Duke Human Vaccine Institute, Duke University School of Medicine, Durham, NC 27710, USA

[2]Department of Medicine, Duke University School of Medicine, Durham, NC 27710, USA

[3]Department of Epidemiology, University of North Carolina at Chapel Hill, Chapel Hill, NC 27599, USA

[4]Infectious Disease Pathogenesis Section, Comparative Medicine Branch, National Institute of Allergy and Infectious Diseases, National Institutes of Health, Bethesda, MD 20892, USA.

[5]Department of Surgery, Duke University, Durham, NC 27710, USA

[6]Ragon Institute of MGH, MIT and Harvard, Cambridge, MA 02139, USA

[7]Department of Pediatrics, Duke University School of Medicine, Durham, NC 27710, USA

[8]Center for Applied Genomics and Precision Medicine, Duke University Medical Center, Durham, NC 27710, USA

[9]Department of Microbiology, Harvard Medical School, Boston, MA 02115, USA

[10]Vaccine Research Center, National Institute of Allergy and Infectious Diseases (NIAID), NIH, Bethesda, MD 20892, USA

[11]Department of Biochemistry and Molecular Biophysics, Columbia University, New York, NY 10032, USA

[12]BIOQUAL, Rockville, MD 20850, USA

[13]Department of Immunology, Duke University School of Medicine, Durham, NC 27710, USA

[14]Department of Molecular Genetics and Microbiology, Duke University School of Medicine, Durham, NC 27710, USA

[*]Co-First Authors

[#]Correspondence: barton.haynes@duke.edu (B.F.H.) and kevin.saunders@duke.edu (K.O.S.)

Summary (135 words)

SARS-CoV-2 neutralizing antibodies (NAbs) protect against COVID-19, making them a focus of vaccine design. A safety concern regarding SARS-CoV-2 antibodies is whether they mediate disease enhancement. Here, we isolated potent NAbs against the receptor-binding domain (RBD) and the N-terminal domain (NTD) of SARS-CoV-2 spike protein from individuals with acute or convalescent SARS-CoV-2 or a history of SARS-CoV-1 infection. Cryo-electron microscopy of RBD and NTD antibodies demonstrated function-specific modes of antibody binding. Select RBD NAbs also demonstrated Fc receptor-γ (FcγR)-mediated enhancement of virus infection *in vitro*, while five non-neutralizing NTD antibodies mediated FcγR-independent *in vitro* infection enhancement. However, both *in vitro* neutralizing and infection-enhancing RBD or infection-enhancing NTD antibodies protected from SARS-CoV-2 challenge in non-human primates and mice. One of 30 monkeys infused with enhancing antibodies had lung pathology and bronchoalveolar lavage cytokine evidence suggestive of enhanced disease. Thus, these *in vitro* assessments of enhanced antibody-mediated infection do not necessarily indicate biologically relevant *in vivo* infection enhancement.

Keywords

SARS-CoV-2, COVID-19, neutralizing antibody, receptor-binding domain, N-terminal domain, electron micrograph, *in vivo* protection, infection enhancement

Introduction

The severe acute respiratory syndrome coronavirus 2 (SARS-CoV-2) has caused a global pandemic with over 43 million cases and 1.16 million deaths (https://coronavirus.jhu.edu/). Development of combinations of neutralizing antibodies for prevention or treatment of infection can significantly help to control the pandemic, while the ultimate solution to control the COVID-19 pandemic is a safe and effective vaccine (Graham, 2020; Sempowski et al., 2020).

Neutralizing antibodies (NAbs) that can block viral entry are crucial for controlling virus infections (Battles and McLellan, 2019; Corti and Lanzavecchia, 2013; Dashti et al., 2019). Previously reported SARS-CoV and MERS-CoV NAbs function by targeting the receptor-binding domain (RBD) or the N-terminal domain (NTD) of spike (S) protein to block receptor binding, or by binding to the S2 region of S protein to interfere with S2-mediated membrane fusion (Du and Jiang, 2010; Jiang et al., 2020; Xu et al., 2019). Importantly, prophylactic or therapeutic use of SARS-CoV-2 NAbs in non-human primates (Shi et al., 2020) or rodent models (Hassan et al., 2020; Rogers et al., 2020; Wu et al., 2020b) showed protection from SARS-CoV-2-induced lung inflammation and/or reduction in viral load. SARS-CoV-2 NAbs reported to date predominantly target the RBD region (Baum et al., 2020; Brouwer et al., 2020a; Cao et al., 2020; Chen et al., 2020; Hansen et al., 2020; Ju et al., 2020; Liu et al., 2020a; Pinto et al., 2020; Robbiani et al., 2020; Rogers et al., 2020; Shi et al., 2020; Wang et al., 2020a; Wrapp et al., 2020a; Wu et al., 2020b). In contrast, NTD antibodies that neutralize SARS-CoV-2 are rare and of modest neutralization potency (Brouwer et al., 2020b; Chi et al., 2020; Wec et al., 2020; Zost et al., 2020a; Zost et al., 2020b).

Antibody-dependent enhancement (ADE) of infection *in vitro* has been reported with a number of viruses. ADE has been associated with vaccination for respiratory syncytial virus (RSV), with vaccination for dengue virus, or with dengue virus infection (Arvin et al., 2020). ADE is often mediated by Fc receptors for IgG (FcγRs), complement receptors (CRs) or both, and is most commonly observed in cells of monocyte/macrophage and B cell lineages (Iwasaki and Yang, 2020; Ubol and Halstead, 2010). *In vitro* studies have demonstrated FcγR-mediated ADE of SARS-CoV-1 infection of ACE2-negative cells (Jaume et al., 2011; Kam et al., 2007; Wan et al., 2020; Wang et al., 2014; Yilla et al., 2005; Yip et al., 2016; Yip et al., 2014). One group demonstrated FcγR-independent infection enhancement of SARS-CoV-1 in Vero cells, and isolated a monoclonal antibody that was suggested to induce enhanced lung viral load and pathology *in vivo* (Wang et al., 2016). The ability of antibodies that bind the

SARS-CoV-2 S protein to mediate infection enhancement *in vivo* is unknown but is a theoretical concern for COVID-19 vaccine development (Arvin et al., 2020; Bournazos et al., 2020; Iwasaki and Yang, 2020).

Here, we identified potent *in vitro* neutralizing RBD and NTD antibodies as well as *in vitro* infection-enhancing RBD and NTD antibodies from individuals infected with SARS-CoV-1 or SARS-CoV-2. Negative stain electron microscopy (NSEM) and cryo-electron microscopy (cryo-EM) revealed distinct binding patterns and the precise epitopes of infection-enhancing and neutralizing antibodies. *In vitro* studies using human FcγR-expressing or ACE2-expressing cell lines demonstrated that the RBD antibodies mediated FcγR-dependent infection enhancement, whereas the NTD antibodies induced FcγR-independent infection enhancement. However, using monkey and mouse models of SARS-CoV-2 infection, none of these infection-enhancing antibodies consistently augmented SARS-CoV-2 lung viral load, infectious virus in the lung, or lung disease pathology *in vivo*. Rather, one of 30 monkeys had lung pathology and bronchoalveolar lavage (BAL) cytokine levels suggestive of enhanced lung disease. *In vitro* infection-enhancing antibodies prevented or reduced virus replication in cynomolgus macaques or mice challenged with SARS-CoV-2, SARS-CoV-2 mouse-adapted (MA) viruses (Dinnon et al., 2020b; Leist et al., 2020a), or bat WIV1-coronavirus (CoV) (Menachery et al., 2016). Thus, the *in vitro* infection enhancing activity of SARS-CoV-2 RBD and NTD antibodies only rarely translated to *in vivo* relevance.

RESULTS

Isolation of infection-enhancing SARS-CoV-2 antibodies

SARS-CoV-2-reactive human monoclonal antibodies from plasmablasts or SARS-CoV-2-reactive memory B cells were isolated by flow cytometric sorting (Liao et al., 2009; Liao et al., 2013) from a SARS-CoV-2 infected individual 11, 15, 36, and 70 days post-onset of symptoms. Additional memory B cells were isolated from an individual infected with SARS-CoV-1 ~17 years prior to sample collection (***Figures 1A-B, S1 and S2***). We isolated and characterized 1,737 antibodies, which bound to SARS-CoV-2 S and nucleocapsid (NP) proteins (***Figure 1C; Table S1***). We selected 187 antibodies for further characterization, and first examined neutralization of SARS-CoV-2 pseudovirus and replication-competent SARS-CoV-2. Forty-four of 81 recombinant RBD antibodies exhibited neutralization when assayed in 293T/ACE-2 cell pseudovirus, SARS-CoV-2 microneutralization, or SARS-CoV-2 plaque reduction assays (***Figures S3A-F; Tables S2-S3***).

Ten of the forty-one NTD antibodies neutralized in the 293T/ACE2 pseudovirus and plaque reduction assays, with the most potent antibody neutralizing pseudovirus with an IC_{50} of 39 ng/mL (***Figures S3G-I; Tables S4-S5***). In addition, 5 non-neutralizing NTD antibodies enhanced SARS-CoV-2 pseudovirus infection in 293T/ACE2 cells by 56% to 148% (***Figure 1D***). To determine whether this effect was applicable to replication-competent virus, we tested these five antibodies for enhancement of SARS-CoV-2 virus infection of Vero cells. Infection of replication-competent SARS-CoV-2 nano-luciferase virus (Hou et al., 2020) also increased in the presence of each of the 5 NTD antibodies (***Figure 1E***). Analysis of *in vitro* enhancement of NTD antibodies in ACE2-negative TZM-bl cells demonstrated no infection enhancement, suggesting enhancement-dependence on ACE2. Both ACE2-expressing 293T cells used for pseudovirus assays and Vero cells lack FcγR expression (Takada et al., 2007). Thus, NTD enhancement of SARS-CoV-2 infection was FcγR-independent.

Previous studies have demonstrated FcγR-mediated ADE of SARS-CoV-1 infection in ACE2-negative cells (Jaume et al., 2011; Kam et al., 2007; Wan et al., 2020; Wang et al., 2014; Yilla et al., 2005; Yip et al., 2016; Yip et al., 2014). Here, FcγR-dependent infection enhancement was determined by generating stable TZM-bl cell lines that expressed individual human FcγRs (FcγRI, FcγRIIa, FcγRIIb or FcγRIII). TZM-bl cells naturally lack ACE-2 and TMPRSS2 receptors, thus SARS-CoV-2 was unable to infect FcγR-negative TZM-bl cells (***Figure 1F***). One hundred S-reactive IgG1 antibodies selected from ***Tables S2-S7*** were tested for their ability to facilitate SARS-CoV-2 infection of TZM-bl cells. Three of the antibodies enabled SARS-CoV-2 infection of TZM-bl cells expressing FcγRI, and five antibodies mediated infection of FcγRIIb-expressing TZM-bl cells (***Figures 1F-J***). The antigen-binding fragments (Fabs) of these antibodies did not mediate infection enhancement of TZM-bl cells expressing FcγRI or FcγRIIb (***Figures 1K-L***). FcγRI and FcγRIIb-dependent infection-enhancing antibodies were specific for the RBD of S protein, consistent with a recent finding by another group using COVID-19 patient sera or a recombinant antibody (Wu et al., 2020a). Thus, RBD antibodies can be either neutralizing in the 293T/ACE2 cell line, infection-enhancing in the TZM-bl-FcγR-expressing cell lines, or both (***Figure 2A***). NTD antibodies can either be neutralizing or infection-enhancing in the 293T/ACE2 cell line or Vero E6 cells (***Figure 2A***). Therefore, the repertoire of SARS-CoV-2 antibodies included potent neutralizing RBD and NTD antibodies, FcγR-dependent, infection-enhancing RBD antibodies, and FcγR-independent infection-enhancing NTD antibodies.

Characterization of infection-enhancing Spike recombinant antibodies

We compared the phenotypes and binding modes to S protein for five infection-enhancing RBD antibodies and three RBD antibodies that lacked infection enhancement to elucidate differences between these two types of antibodies. All selected RBD antibodies neutralized SARS-CoV-2 pseudovirus and/or replication-competent virus in ACE2-expressing cells (***Figures 2A and S5***), despite five of these antibodies mediating infection enhancement in ACE2-negative, FcγR-positive TZM-bl cells (***Figures 1F-L, 2A,and S5***). Both types of selected RBD antibodies blocked ACE2 binding to S protein. Fabs of four of the infection-enhancing RBD antibodies and two of the non-infection-enhancing RBD antibodies bound to S with high affinities ranging from 0.1 to 9 nM (***Figures S6-8***). Thus, the infection-enhancing or non-enhancing RBD antibodies showed similarities in ACE2 blocking, affinity, and neutralization of ACE2-dependent SARS-CoV-2 infection (***Figure 2A***).

We obtained NSEM reconstructions of Fabs in complex with stabilized S ectodomain trimer for six representative RBD antibodies (Hsieh et al., 2020). Infection-enhancing RBD antibodies DH1041 and DH1043 bound with a vertical approach (***Figure 2B***), parallel to the central axis of the S trimer, similar to non-infection-enhancing antibodies DH1042 and DH1044 (***Figure 2C***). The epitopes of antibodies DH1041, DH1042, and DH1043 overlapped with that of the ACE-2 receptor (Wang et al., 2020b), consistent with their ability to block ACE-2 binding to S protein (***Figure 2A and S10***). Their epitopes were similar to those of three recently described antibodies, P2B-2F6 (Ju et al., 2020), H11-H4, and H11-D4 (***Figure S10***) (Huo et al., 2020; Zhou et al., 2020). The epitope of another non-infection-enhancing RBD antibody DH1044 was only slightly shifted relative to DH1041, DH1042 and DH1043 (***Figure 2C***), but resulted in DH1044 not blocking ACE2 binding (***Figure 2A and S10***). The remaining two RBD antibodies, DH1045 and DH1047 cross-reacted with both SARS-CoV-1 and SARS-CoV-2 S (***Figure 2A and S4***). Although DH1047 mediated FcγR-dependent infection of TZM-bl cells and DH1045 did not, both antibodies bound to RBD-up S conformations with a more horizontal angle of approach (***Figure 2B-C and S10***) (Pak et al., 2009). Thus, epitopes and binding angles of RBD antibodies determined by NSEM did not discriminate between antibodies that mediated FcγR-dependent infection enhancement and those that did not.

We performed similar comparative analyses of five FcγR-independent, infection-enhancing NTD antibodies, and five non-infection-enhancing NTD antibodies (DH1048, DH1049, DH1051, DH1050.1 and DH1050.2) that neutralized SARS-CoV-2 (pseudovirus IC_{50} titers 39 - 520 ng/mL; SARS-CoV-2 plaque reduction IC_{50} titers 390 -

780 ng/mL) (***Figure 2A and S5C-D***). The Fabs of neutralizing antibodies DH1050.1 and DH1051 bound to stabilized S ectodomain with affinities of 16 and 19 nM respectively, whereas the infection-enhancing antibody DH1052 bound with 294 nM affinity (***Figures S6-8***). NSEM reconstructions obtained for nine of the ten NTD antibodies showed that the FcγR-independent, infection-enhancing NTD antibodies (DH1053-DH1056) bound to S with their Fab constant domains directed downward toward the virus membrane (***Figure 2D)***, whereas the five neutralizing NTD-directed Abs (DH1048-DH1051) bound to S with the constant domain of the Fab directed upward away from the virus membrane (***Figure 2E)***. Thus, S protein antibody epitopes and binding modes were associated with FcγR-independent, infection-enhancing activity of NTD antibodies. The five neutralizing antibodies bound the same epitope as antibody 4A8 (Wrapp et al., 2020a), with three of the five having the same angle of approach as 4A8 (***Figure S11***). Interestingly, the NTD antibodies with the same angle of approach as 4A8, were also genetically similar to 4A8, being derived from the same V_H1-24 gene segment (***Table S8***), although their light chains were different (Wrapp et al., 2020a). These antibodies may constitute a neutralizing antibody class that can be reproducibly elicited upon SARS-CoV-2 infection.

Competition between infection-enhancing and non-infection enhancing antibodies

To determine whether infection-enhancing antibodies could compete with non-infection-enhancing antibodies for binding to S ectodomain, we performed surface plasmon resonance (SPR) competitive binding assays. RBD antibodies segregated into two clusters, where antibodies within a cluster blocked each other and antibodies in different clusters did not block each other (***Figures 3A and S12***). One cluster included antibodies DH1041, DH1043 and DH1044, and the other cluster included antibodies DH1046 and DH1047. NSEM reconstructions showed DH1041 and DH1047 Fabs bound simultaneously to different epitopes of the stabilized S trimer (***Figure 3B***). Similarly, DH1043 and DH1047 Fabs also bound simultaneously to different epitopes on the stabilized S protein (***Figure 3B***).

NTD antibodies also segregated into two clusters based on their ability to block each other (***Figure 3A***). Neutralizing NTD antibodies blocked each other and formed one cluster, while infection-enhancing/non-neutralizing NTD antibodies blocked each other and formed a second cluster (***Figures 3A, 3C, S12 and S13***). NSEM reconstruction of SARS-CoV-2 S trimer bound with Fabs of neutralizing NTD antibody DH1050.1 and

infection-enhancing NTD antibody DH1052 confirmed that the two antibodies could simultaneously bind to distinct epitopes on a single SARS-CoV-2 S trimer (***Figure 3D***). DH1054 was unique as it was able to block both infection-enhancing and neutralizing NTD antibodies (***Figures 3C and S13***).

NTD antibodies did not compete with RBD antibodies for binding to S trimer (***Figure 3A***). This result gave rise to the notion that in a polyclonal mixture of antibodies, the SARS-CoV-2 S trimer could bind both RBD and NTD antibodies. To determine the potential for this complex to form, we liganded SARS-CoV-2 S trimer with Fabs of each type of antibody and visualized the complex using NSEM. NSEM showed that neutralizing RBD antibodies could also bind to the same S protomer as neutralizing NTD antibodies DH1050.1 or DH1051 (***Figure 3E***). Moreover, we found that a single S protomer could be simultaneously occupied by two RBD antibodies (DH1043 and DH1047) and an NTD antibody (DH1050.1) (***Figure 3F***). Thus, the S trimer could simultaneously bind to multiple RBD and NTD neutralizing antibody Fabs.

FcγR-independent infection-enhancement in the presence of neutralizing antibodies

The NSEM determination of antibody binding modes demonstrated that certain infection-enhancing antibodies and non-infection enhancing antibodies bound to distinct epitopes on the same S protomer (***Figures 3A-F***). Thus, we determined the functional outcome of infection-enhancing antibodies binding to S in the presence of neutralizing antibodies. We examined whether a FcγR-independent, infection-enhancing NTD antibody could inhibit RBD antibody neutralization of ACE-2-mediated SARS-CoV-2 pseudovirus infection of 293T/ACE2 cells *in vitro*. We hypothesized that the outcome would be dependent on which antibody was present at the highest concentration. We examined RBD antibody DH1041 neutralization in the presence of 132 and 1,325-fold excess of infection-enhancing NTD antibody DH1052. DH1041 neutralization activity was minimally decreased in the presence of 132-fold excess of DH1052. When DH1041 neutralization was assessed in the presence of 1,325-fold excess of antibody DH1052, infection enhancement was observed when DH1041 concentration was below 10 ng/mL (***Figures 3G and S14***). A nearly identical result was obtained when we examined neutralization by DH1043 (***Figures 3H and S14***). Thus, a ~1000-fold excess of infection-enhancing NTD antibody was required to out-compete the effect of a potent RBD neutralizing antibody *in vitro*.

Cryo-EM structural determination of RBD and NTD-directed antibody epitopes

To visualize atomic level details of their interactions with the S protein, we selected representatives from the panels of RBD and NTD-directed antibodies for structural determination by cryo-EM. Of the RBD-directed antibodies, we selected two (DH1041 and DH1043) that most potently neutralized SARS-CoV-2 virus in the 293T/ACE2 pseudovirus assay and also enhanced infection in TZM-bl-FcγRI or -FcγRIIb cells. We also selected the RBD-directed antibody DH1047, which shared the infection enhancing and ACE-2 blocking properties of DH1041 and DH1043, but unlike DH1041 and DH1043, DH1047 also showed reactivity with the SARS-CoV-1 S protein. From the panel of NTD-directed antibodies, we selected one infection-enhancing NTD antibody, DH1052, and one neutralizing NTD antibody, DH1050.1, for higher resolution structural determination by cryo-EM. The stabilized SARS-CoV-2 S ectodomain "2P" (S-2P) (Wrapp et al., 2020b) was used for preparing complexes for structural determination.

For all three RBD-directed antibodies, the cryo-EM datasets revealed heterogeneous populations of S protein with at least one RBD in the "up" position (***Figures 4, S15 and S16***). We did not find any unliganded S or any 3-RBD-down S population, even though the unliganded S-2P consistently shows a 1:1 ratio of 1-RBD-up and 3-RBD-down populations (Henderson et al., 2020; Walls et al., 2020), suggesting that binding of the RBD-directed antibodies to S protein alters RBD dynamics. All S-2P trimers were stoichiometrically bound to 3 Fabs, with antibodies bound to both up and down RBDs in an S-2P trimer.

We observed that the primary epitopes of DH1041 and DH1043 were centered on the Receptor Binding Motif (RBM; residues 483-506) of the RBD (***Figures 4A-B, S17 and S18***), providing structural basis for the ACE-2 blocking phenotype of these antibodies. While DH1041 utilized its heavy chain complementarity determining regions (CDRs) to contact the RBM, the DH1043 paratope included both its heavy and light chains.

Unlike the RBM-focused epitope of DH1041 and DH1043, the epitope of antibody DH1047 was focused around the α2 and α3 helices and ß2 strand that are located outside the N-terminus of the RBM (***Figures 4C and S19***)(Ju et al., 2020). Contact is also made by RBD residues 500-506 that are also outside the RBM but at its C-terminal end, and stack against the N-terminal end of the α3 helix providing a continuous interactive surface for DH1047 binding. The DH1047 paratope included heavy chain complementarity determining regions HCDR2, HCDR3 and light chain LCDR1 and LCDR3. The HCDR3 stacks against and interacts with the residues in the ß2 strand. Interactions with the ß2 strand are also mediated by HCDR2. Similar to DH1041 and DH1043, the DH1047

interacted with an "up" RBD conformation from an adjacent protomer although these interactions were not well-characterized due to disorder in that region.

We next determined cryo-EM structures of the NTD-directed neutralizing antibodies, DH1050.1 (***Figure 4D***) and NTD-directed infection-enhancing antibody, DH1052 (***Figure 4E***), at 3.4 Å and 3.0 Å resolutions, respectively. Unlike the RBD-directed antibodies DH1041, DH1043 and DH1047, where we only observed spikes with at least one RBD in the up position, the cryo-EM datasets of DH1050.1- and DH1052-bound complexes showed antibody bound to both 3-RBD-down and 1-RBD-up S-2P spikes (***Figures S20-S21***). Consistent with the NSEM reconstructions, the neutralizing antibody DH1050.1 and the non-neutralizing, infection-enhancing antibody DH1052 bound opposite faces of the NTD, with the epitope for the neutralizing antibody DH1050.1 facing the host cell membrane and the epitope for the non-neutralizing, infection-enhancing antibody DH1052 facing the viral membrane. The dominant contribution to the DH1050.1 epitope came from NTD loop region 140-158 that stacks against the antibody HCDR3 and extends farther into a cleft formed at the interface of the DH1050.1 HCDR1, HCDR2 and HCDR3 loops. The previously described NTD antibody 4A8 interacts with the same epitope in a similar elongated HCDR3-dominated manner making similar contacts, although DH1050.1 and 4A8 (Chi et al., 2020) show a rotation about the stacked HCDR3 and NTD 140-158 loops, suggesting focused recognition of the elongated NTD loop by a class of antibodies sharing the same VH origin. Consistent with their diverse light chain gene origins, the light chains of DH1050.1 and 4A8 do not contact the S protein. The focused recognition of the NTD loop 140-158 by DH1050.1 is reminiscent of the interactions that HIV-1 fusion peptide-directed antibodies make with the HIV-1 Env, where recognition is focused on the conserved region of the flexible fusion peptide (Dingens et al., 2018; Xu et al., 2018). In a structurally conserved mechanism, such focused recognition is characterized by robust cryo-EM density at the recognition site but increased disorder away from the site of focused interactions (***Figures 4E and S21)***.

The infection enhancing NTD-directed antibody DH1052 bound the NTD at an epitope facing the viral membrane and comprised of residues spanning 27-32, 59-62 and 211-218, with all the CDR loops of both heavy and light chains involved in contacts with the NTD. We also observed contact of the antibody with the glycan at position 603, as well as the conformationally invariant SD2 region.

Thus, we found that the RBD-directed antibodies isolated in this study influenced RBD dynamics and bound only to spike with at least one RBD in the up conformations, and in some cases, also induced the 2-RBD-up and 3-

RBD-up spike conformations. In contrast, the NTD-directed antibodies bound to both the 3-RBD-down and 1-RBD-up spikes that are present in the unliganded S-2P. Our results provide a structural explanation for the ACE-2 blocking activity of RBD-directed antibodies as well as for the cross-reactivity of the DH1047 antibody. We observed two distinct orientations for the NTD-directed antibodies that are either neutralizing or non-neutralizing, with the former binding the NTD surface that faces away from the viral membrane and the latter binding the surface that faces the viral membrane.

NTD antibodies that mediate SARS-CoV-2 infection enhancement *in vitro*, do not necessarily enhance infection or disease in murine and macaque models of infection

To determine the biological relevance of *in vitro* infection enhancement by NTD antibodies, we assessed enhanced SARS-CoV-2 acquisition or disease severity *in vivo* in a COVID-19 disease mouse model of aged BALB/c mice challenged with the mouse-adapted SARS-CoV-2 MA10 strain (Leist et al., 2020a). The FcγR-independent, *in vitro* infection-enhancing antibody DH1052 or a control influenza antibody CH65 were given 12 hours prior to SARS-CoV-2 MA10 infection (***Figure 5A***). Throughout the four days of infection, DH1052-infused mice exhibited similar levels of body weight loss and higher survival than mice given negative control IgG (2/9 control mice died while 0/10 DH1052-treated mice died) (***Figures 5B-C***). In addition, DH1052-treated mice exhibited lower lung hemorrhagic scores, lower lung viral titers and lower lung tissue subgenomic RNA levels compared to control IgG-infused mice (***Figures 5D-F***). Overall, DH1052 treatment resulted in less severe disease and reduced viral replication rather than infection enhancement. Therefore, NTD antibodies that enhanced infection *in vitro* did not enhance infection or disease *in vivo* in the SARS-CoV-2 MA10 virus infection mouse model.

Next, we examined the effect of infusion of NTD antibody DH1052 on SARS-CoV-2 infection in monkeys (Leist et al., 2020b; Rockx et al., 2020). Cynomolgus macaques were infused with 10 mg of antibody per kilogram of body weight and then challenged intranasally and intratracheally with 10^5 plaque forming units of SARS-CoV-2 three days later (***Figure 5G***) (54). We compared the protective activity of *in vitro* infection-enhancing antibody DH1052, neutralizing NTD antibody DH1050.1, and negative control influenza antibody CH65 in separate groups of macaques. While no human antibody was detected pre-infusion (***Figure 5H***), antibody infusion resulted in human antibody concentrations ranging from 11 to 238 μg/mL in serum at day 2 post-challenge (***Figure 5I and S26A-D***). Sera with DH1050.1 neutralized SARS-CoV-2 pseudovirus at a mean ID_{50} titer of 19 (***Figure 5J***), and

304 neutralized SARS-CoV-2 replication-competent virus at a mean ID_{50} titer of 192 (***Figure 5K***). In contrast, the
305 presence of DH1052 or control antibody CH65 in serum did not neutralize SARS-CoV-2 (***Figure 5J-K***).
306 Macaques that received CH65 or DH1052 had comparable lung inflammation four days after infection (***Figures***
307 ***5L, S22 and S23A***). However, one macaque administered DH1052 showed increased perivascular mononuclear
308 inflammation, perivascular and alveolar edema (***Figure S23B***), and multiple upregulated bronchoalveolar fluid
309 (BAL) cytokines (***Figure S24-S25***) compared to either control antibody-infused animals or the four other monkeys
310 in the DH1052-treated group. In contrast, macaques administered DH1050.1, a neutralizing NTD antibody, had
311 lower lung inflammation than CH65-infused macaques (***Figures 5L, S22 and S23A)***. Infusion of either neutralizing
312 NTD DH1050.1 or *in vitro* infection-enhancing antibody DH1052 reduced viral nucleocapsid antigen in the lung
313 (***Figures 5M, S22 and S23A)***. Envelope (E) gene subgenomic RNA (sgRNA) and nucleocapsid (N) gene sgRNA
314 in the BAL were also reduced in macaques that were administered DH1050.1 or DH1052 compared to macaques
315 treated with negative control antibody (***Figures 5N-O and S26G***). In nasal swab fluid, macaques showed reduced E
316 and N gene sgRNA when DH1050.1 or DH1052 was infused respectively, with the reduction by DH1050.1 being
317 statistically significant (***Figures 5P-Q, S26E-F and S26H-I***). Thus, neutralizing NTD antibody DH1050.1
318 provided protection against SARS-CoV-2 infection in cynomolgus macaques, while the *in vitro* infection-
319 enhancing antibody DH1052 showed no infection enhancement overall, but rather showed partial protection from
320 SARS-CoV-2 infection.
321
322 **FcγR-dependent, *in vitro* infection-enhancing RBD antibodies do not enhance SARS-CoV-2 infection in mice**
323 We next tested RBD neutralizing antibodies that also mediated infection enhancement in TZM-bl cells
324 expressing FcγRI or FcγRII in a SARS-CoV-2 acquisition mouse model (***Figures 6A-B***). Aged (12 months old)
325 BALB/c mice were injected intraperitoneally with 300 μg of antibody, and challenged with a SARS-CoV-2 mouse-
326 adapted (MA) isolate twelve hours later (Dinnon et al., 2020a). Mice received either FcγR-dependent, *in vitro*
327 infection-enhancing antibody DH1041, non-infection enhancing antibody DH1050.1, or a combination of both
328 antibodies. Administration of RBD NAb DH1041 alone or in combination with DH1050.1 protected all mice from
329 detectable infectious virus in the lungs 48h after challenge (***Figure 6A***). In the setting of therapeutic treatment,
330 administration of DH1041 alone (300 μg) or in combination with DH1050.1 (150 μg of each) twelve hours after

SARS-CoV-2 challenge significantly reduced lung infectious virus titers, with half of the mice having undetectable infectious virus in the lung 48h after challenge (***Figure 6B***). Thus, while RBD antibody DH1041 could mediate FcγR-dependent, *in vitro* infection enhancement, it protected mice from SARS-CoV-2 infection when administered prophylactically or therapeutically.

DH1046 and DH1047 are RBD antibodies that neutralize SARS-CoV, SARS-CoV-2 and bat WIV1-CoV (Menachery et al., 2016) (***Figure 2A***, ***S4A-B, S5E-H and S27***). Both of these RBD antibodies mediated FcγR-dependent, *in vitro* SARS-CoV-2 infection enhancement of TZM-bl cells that lacked ACE-2 expression (***Figures 1F-L***). To determine whether SARS-CoV-2 *in vitro* infection enhancement predicted *in vivo* infection enhancement by SARS-related bat coronaviruses, we assessed the ability of either DH1046 or DH1047 to enhance or protect against bat WIV1-CoV infection in HFH4-ACE2-transgenic mice. Mice were challenged either 12 hours before or 12 hours after intraperitoneal injection of antibody (***Figures 6C-D***). Mice administered DH1046 or DH1047 before challenge had no detectable infectious virus in the lung, whereas control IgG administered mice had a mean titer of 84,896 plaque forming units per lung lobe (***Figure 6C***). Administration of DH1047 after challenge eliminated detectable infectious virus in the lung in 3 of 5 mice (***Figure 6D***). Therapeutic administration of DH1046 reduced infectious virus titers 10-fold compared to negative control IgG (***Figure 6D***). Thus, FcγR-dependent *in vitro* infection-enhancing RBD antibodies DH1046 and DH1047 did not enhance infection *in vivo*, but rather protected mice from SARS-related bat coronavirus infection.

In vitro infection-enhancing RBD antibodies do not enhance SARS-CoV-2 infection in nonhuman primates

Finally, we assessed the *in vivo* relevance of RBD antibody infection enhancement in the cynomolgus macaque SARS-CoV-2 intranasal/intratracheal challenge model. We examined *in vivo* infection enhancement by RBD antibodies DH1041, DH1043, DH1046, and DH1047 that neutralized SARS-CoV-2 pseudovirus and replication-competent virus, but enhanced infection *in vitro* in FcγRI or FcγRIIb-expressing TZM-bl cells (***Figures 1 and 6E***). After antibody infusion at 10 mg of antibody per kg of macaque body weight, serum human IgG concentrations reached 11-228 μg/mL at day 2 post-challenge (***Figure 6F-G and S26A-D***). The same macaque serum containing the RBD antibodies exhibited a wide range of neutralization potency (ID_{50} titers) against SARS-CoV-2 pseudovirus or replication-competent virus, commensurate with the neutralization potency of each antibody

(***Figure 6H and 6I***). Infusion of RBD antibody DH1041, DH1043, or DH1047 resulted *in vivo* protection from SARS-CoV-2 infection. In macaques administered DH1041, DH1043, or DH1047, lung inflammation was reduced and lung viral antigen was undetectable in all but one macaque (***Figures 6J-K, S22 and S23A***). E gene sgRNA and N gene sgRNA were significantly reduced in the upper and lower respiratory tract based on analyses of bronchoalveolar lavage fluid, nasal swabs, and nasal wash samples (***Figures 6L-O and S26E-I***). The RBD antibody DH1046 only protected a subset of infused monkeys. Four monkeys treated with RBD antibody DH1046 exhibited the same or lower levels of lung inflammation compared to monkeys that received control IgG (***Figure 6J***). One DH1046-infused monkey had an increased lung inflammation score compared to control antibody monkeys (***Figures 6J, S22, and S23***), but had not evidence of perivascular or alveolar edema or evidence of abnormal BAL cytokines (***Figures S24-S25***). Comparing the DH1046 group to the control IgG group, viral antigen in the lung was reduced overall (***Figures 6K, S22 and S23A***), however reductions in E gene and N gene sgRNA levels were not significant in BAL or nasal fluid at most timepoints (***Figures 6L-O and S26E-I***). These results further demonstrated that both FcγR-independent and FcγR-dependent *in vitro* SARS-CoV-2 infection enhancement did not translate to SARS-CoV-2 *in vivo* infection enhancement.

DISCUSSION

Antibody enhancement of virus infection *in vitro* has been reported for MERS-CoV and SARS-CoV (Gu et al., 2005; Liu et al., 2020a; Wan et al., 2020; Wang et al., 2016) and is a critical question facing the safe administration of antibody prophylaxis, antibody therapy, and antibody-based COVID-19 vaccines (Halstead and Katzelnick, 2020; Karthik et al., 2020; Lee et al., 2020; Ulrich et al., 2020). The effects of SARS-CoV-2 antibodies have been further questioned since individuals who seroconverted earlier tend to have more severe COVID-19 disease than later seroconverters (Ho et al., 2005). Here, we demonstrated that SARS-CoV-2 antibodies can mediate infection enhancement *in vitro*. However, this *in vitro* phenotype does not translate to enhanced SARS-CoV-2 or SARS-related virus infection in mice, nor does it usually translate to enhanced infection in a non-human primate model of SARS-CoV-2 infection. We assessed *in vivo* infection enhancement as severe lung immunopathology or increased respiratory tract virus replication. Neither of these hallmarks of infection enhancement was significantly present in mice. Two of 30 monkeys administered RBD or NTD antibodies that mediate infection enhancement *in vitro* had increased lung inflammation despite having low or undetectable lung viral antigen. One of these two macaques had

lung histology and BAL cytokine levels suggestive of antibody-mediated enhanced pathology. However, these indicators of antibody-mediated enhancement were not present in all macaques that received the same antibody, thus host-specific differences may have influenced the pathology outcomes. These preclinical results indicate that SARS-CoV-2 antibody treatments or the induction of SARS-CoV-2 antibodies by vaccination have a low likelihood of exacerbating COVID-19 disease in humans.

It is of interest that a potent therapeutic Spike antibody, LY-CoV555 recently failed to demonstrate efficacy in the treatment of hospitalized patients with COVID-19 (ACTIV-3/TICO LY-CoV555 Study Group,(2020). We observed here that high levels (1,345-fold excess) of enhancing antibodies can overcome effects of neutralizing antibodies and enhance SARS-CoV-2 infection *in vitro* (***Figure S14***). It will be of interest to determine if the lack of efficacy was due to neutralizing effects of LY-CoV555 being outcompeted by infection-enhancing effects of host antibodies.

Previous studies with polyclonal serum antibodies against SARS-CoV have also shown *in vitro* FcγR-dependent infection enhancement, but no *in vivo* infection enhancement in hamsters (Kam et al., 2007). For the present study, there are two potential explanations for why there is a lack of congruence between *in vitro* infection enhancement assays and outcomes of passive antibody infusion/SARS-CoV-2 challenge studies. First, macrophages and other phagocytes are the target cells that uptake MERS-CoV when infection enhancement occurs (Hui et al., 2020; Wan et al., 2020; Zhou et al., 2014). In contrast, SARS-CoV and SARS-CoV-2 do not productively infect macrophages (Bournazos et al., 2020; Hui et al., 2020; Yip et al., 2016). Thus, while RBD antibodies may be able to mediate FcγR-dependent virus uptake of SARS-CoV-2 *in vitro*, *in vivo* FcγR-dependent virus uptake of SARS-CoV-2 may largely lead to abortive infection in macrophages (Cheung et al., 2005; Yip et al., 2016).

A second potential explanation for a lack of agreement between *in vitro* infection enhancement assays and *in vivo* studies is that *in vivo* SARS-CoV-2 antibodies may have the ability to combat SARS-CoV-2 replication through antibody effector functions. While circulating *in vivo*, antibodies can opsonize infected cells or virions and recruit effector immune cells to kill the virus or the infected cells through Fc-mediated mechanisms. A recent study in a SARS-CoV-2 mouse model of acquisition suggested that Fc effector functions contribute to the protective activity of SARS-CoV-2 neutralizing antibodies C104, C002, and C110 (Schafer et al., 2021). Thus, antibody effector functions may contribute to the outcome *in vivo*, but not be accounted for in SARS-CoV-2 neutralization

assays *in vitro*. In support of this hypothesis, infection-enhancing, non-neutralizing NTD antibody DH1052 reduced infectious virus titers in the lungs of challenged mice compared to the negative control antibody. Consistent with previous findings for human IgG (Dekkers et al., 2017), we have demonstrated that DH1052 antibody can bind to murine FcγRs (Alam SM, Li D, Saunders KO, Haynes BF, unpublished), raising the hypothesis that Fc-mediated effector functions may be responsible for the reduction in infectious virus observed in our mouse challenge study. Future studies will investigate the Fc-mediated effector functions of DH1052 to discern their role in reducing infectious SARS-CoV-2 virus titer *in vitro* and *in vivo*.

Notably, we observed two different types of *in vitro* infection enhancement. First, RBD antibodies mediated classical antibody-dependent enhancement that required FcγRs for virus uptake (Lee et al., 2020). Previous studies have demonstrated that uptake of MERS-CoV or SARS-CoV has mostly been mediated by FcγRIIa on the surface of macrophages (Bournazos et al., 2020; Wan et al., 2020; Yip et al., 2016). In contrast to SARS-CoV and MERS-CoV infection enhancing antibodies, we identified SARS-CoV-2 RBD antibodies utilized FcγRIIb or FcγRI. Thus, different FcγRs can mediate SARS-CoV and MERS-CoV *in vitro* infection enhancement compared to SARS-CoV-2 *in vitro* infection enhancement. Second, non-neutralizing NTD antibodies mediated FcγR-independent infection enhancement in two different FcγR-negative, ACE-2-expressing cell types. The mechanism of this *in vitro* enhancement remains unclear, but one hypothesis is the possibility of antibody modulation of S protein conformation. In NSEM studies, NTD antibodies preferentially bound to S in a 3-RBD-down conformation. One study has reported that binding of select NTD antibodies to S enhances S binding to ACE2 (Liu et al., 2020b). Whether S protein has different entry kinetics or higher affinity for ACE-2 when liganded to infection-enhancing antibody DH1052 will be a focus of future studies.

There are currently over 100 COVID-19 vaccine candidates under development (Anderson et al., 2020; Corbett et al., 2020a; Corbett et al., 2020b; Folegatti et al., 2020; Jackson et al., 2020; Mulligan et al., 2020; Wrapp et al., 2020b). Both the Pfizer/BioNTech and Moderna mRNA-lipid nanoparticle (LNP) vaccine efficacy trials have completed and showed ~95% vaccine efficacy (Jackson et al., 2020; Polack et al., 2020). The Moderna vaccine trial had 30 severe COVID-19 cases—all in the placebo group—indicating no disease enhancement was seen (www.fda.gov, 2020). It is also important to note that administration of COVID-19 convalescent sera to over 35,000 COVID-19 patients have demonstrated the treatment to be safe and is not associated with enhanced disease (Joyner et al., 2020). However, a recent study demonstrated that suboptimal neutralizing antibody level is a

significant predictor of severity for SARS-CoV-2 (Garcia-Beltran et al., 2020). Thus it will be important to continue to monitor on-going COVID-19 vaccine efficacy trials for the possibility of vaccine associated enhanced disease (VAED) (Haynes et al., 2020).

Our results here indicate while SARS-CoV-2 enhancement occurred in SARS-CoV-2 infection assays *in vitro*, these assays did not always predict infection enhancement in mice or monkeys *in vivo*. Additionally, the SARS-CoV-2-infected individual from whom many of our antibodies were isolated did not progress to severe COVID-19 disease. Thus, these results suggest that antibody-induced enhancement of infection is a rare possibility but will not likely be a biologically relevant adverse effect following COVID-19 vaccination in humans.

METHODS

Detailed methods are provided in the supplemental online material.

ACKNOWLEDGMENTS

We thank the COVID-19 donors enrolled in the Molecular and Epidemiological Study of Suspected Infection protocol (MESSI), the MESSI clinical support team, the DHVI Clinical Accessioning Unit Core and the DHVI Immunology and Virology Quality Assessment Core for sample procurement, processing and biobanking. We thank Joseph Gilmore, Steve Slater, Kwan-Ki Hwang, Ahmad Yousef Abuahmad, and the Duke Human Vaccine Institute Flow Cytometry Facility for flow cytometric sorting; Tyler Evangelous for purification of PCR product; Caroline Jones for production of fluorophore-labeled reagents; Kara Anasti and the Duke BMI CORE facility for SPR measurements of antibody affinities; Madison Berry and Sravani Venkatayogi for bioinformatics assistance; Paige Rawls, Lena Smith, Jemma Hwang, Beth Bryan, Jingjing Li, Haiyan Chen for protein and DNA production assistance; Nicole De Naeyer for RNA extraction assistance. We thank Drs. Matthew Gagne and Daniel C. Douek at VRC/NIH for the helpful discussions regarding the subgenomic RNA assays. We thank Kelly Soderberg, Elizabeth Donahue, Amelia Karlsson, Amanda Newman and Whitney Edwards for program management. COVID-19 donor sample processing, flow cytometric sorting, and replication-competent virus neutralization assays were performed in the Duke Regional Biocontainment Laboratory, which received partial support for construction from the National Institutes of Health, National Institute of Allergy and Infectious Diseases (UC6-AI058607). This work was supported by a contract from the State of NC funded by the Coronavirus Aid, Relief, and Economic Security

Act (CARES Act); an administrative supplement to NIH R01 AI145687 for coronavirus research (P.A.); NIH grants R01AI157155 and U54CA260543 (R.S.B.); NIH NIAID U19AI142596 grant (B.F.H.); NIH R01 AI146779 and a Massachusetts Consortium on Pathogenesis Readiness (MassCPR) grant (A.G.S.); training grants: NIGMS T32 GM007753 (B.M.H. and T.M.C); T32 AI007245 (J.F.); and a cooperative agreement with DOD/DARPA (HR0011-17-2-0069; G.D.S). Cryo-EM data were collected at the National Center for Cryo-EM Access and Training (NCCAT) and the Simons Electron Microscopy Center located at the New York Structural Biology Center, supported by the NIH Common Fund Transformative High Resolution Cryo-Electron Microscopy program (U24 GM129539,) and by grants from the Simons Foundation (SF349247) and NY State. We thank Ed Eng, Carolina Hernandez and Daija Bobe for microscope alignments and assistance with cryo-EM data collection. This study utilized the computational resources offered by Duke Research Computing (http://rc.duke.edu; NIH 1S10OD018164-01) at Duke University. David R. Martinez is funded by an NIH F32 AI152296, a Burroughs Wellcome Fund Postdoctoral Enrichment Program Award, and was previously supported by an NIH NIAID T32 AI007151. We thank M. DeLong, C. Kneifel, M. Newton, V. Orlikowski, T. Milledge, and D. Lane from the Duke Office of Information Technology and Research Computing for assisting with setting up and maintaining the computing environment. We thank Laurent Pessaint, Anthony Cook, Alan Dodson, Katelyn Steingrebe and Bridget Bart at BIOQUAL for administrative and technical assistance with non-human primate studies.

AUTHOR CONTRIBUTIONS

D.L. designed and performed experiments, analyzed data, and wrote the manuscript. R.J.E., K.Mansouri, K.Manne, S.G., K.J., M.K., V.S. and P.A. performed structure experiments and analysis. R.J.E. and P.A. supervised structural studies and wrote the manuscript. S.M.A. and K.C. performed and analyzed the SPR work. A.S. and D.R.M. performed the mouse challenge work. D.R.M., L.V.T., T.D.S performed SARS-CoV-1 and bat CoV neutralization assays. K.W. performed bioinformatic analysis of antibody sequences. X.L. performed antibody isolation. R.P., V.G., and M.D. performed ELISA assay. L.L.S. oversaw the NHP study. C.T.D. and T.N.D oversaw the viral RNA assay. T.H.O. and G.D.S. performed SARS-CoV-2 virus neutralization assays. E.L., A.F., F.C., G.E.H., A.S., K.T. and C.J. prepared DNA and produced antibodies. L.G.P., C.M. and D.C.M. performed pseudovirus neutralization assays. M.B., T.V.H. and B.F.H. performed autoreactivity assays. C.W.W and E.P. oversaw setting up the MESSI donor cohort. A.M., E.S., and R.P. performed COVID-19 donor serology. M.A.M.

oversaw the protein fluorescent labeling and flow cytometry sorting. D.W.C. designed and performed flow cytometry sorting. A.G.S., J.F., B.M.H, T.M.C., I.T., T.Z., P.D.K., J.M. and B.G. provided key reagents for this study. K.W.B., M.M., B.M.N., I.N.M., and R.S. oversaw or performed pathology experiments. H.A., and M.G.L. led and performed the non-human primate studies. R.S.B. supervised the SARS-CoV-1 and bat CoV neutralization assays and the mouse challenge studies. K.O.S. and B.F.H. conceived, designed and supervised the study, reviewed all data, and wrote the paper. All authors reviewed and commented on the manuscript.

DECLARATION OF INTERESTS

B.F.H., G.D.S. K.O.S., R.P., D.L. and X.L. have applied for patents concerning SARS-CoV-2 antibodies that are related to this work. All other authors declare no conflict of interest.

REFERENCES

Anderson, E.J., Rouphael, N.G., Widge, A.T., Jackson, L.A., Roberts, P.C., Makhene, M., Chappell, J.D., Denison, M.R., Stevens, L.J., Pruijssers, A.J., *et al.* (2020). Safety and Immunogenicity of SARS-CoV-2 mRNA-1273 Vaccine in Older Adults. N Engl J Med.

Arvin, A.M., Fink, K., Schmid, M.A., Cathcart, A., Spreafico, R., Havenar-Daughton, C., Lanzavecchia, A., Corti, D., and Virgin, H.W. (2020). A perspective on potential antibody-dependent enhancement of SARS-CoV-2. Nature *584*, 353-363.

Battles, M.B., and McLellan, J.S. (2019). Respiratory syncytial virus entry and how to block it. Nat Rev Microbiol *17*, 233-245.

Baum, A., Fulton, B.O., Wloga, E., Copin, R., Pascal, K.E., Russo, V., Giordano, S., Lanza, K., Negron, N., Ni, M., *et al.* (2020). Antibody cocktail to SARS-CoV-2 spike protein prevents rapid mutational escape seen with individual antibodies. Science *369*, 1014-1018.

Bournazos, S., Gupta, A., and Ravetch, J.V. (2020). The role of IgG Fc receptors in antibody-dependent enhancement. Nat Rev Immunol *20*, 633-643.

Brouwer, P.J.M., Caniels, T.G., van der Straten, K., Snitselaar, J.L., Aldon, Y., Bangaru, S., Torres, J.L., Okba, N.M.A., Claireaux, M., Kerster, G., *et al.* (2020a). Potent neutralizing antibodies from COVID-19 patients define multiple targets of vulnerability. Science *369*, 643-650.

Brouwer, P.J.M., Caniels, T.G., van der Straten, K., Snitselaar, J.L., Aldon, Y., Bangaru, S., Torres, J.L., Okba, N.M.A., Claireaux, M., Kerster, G., *et al.* (2020b). Potent neutralizing antibodies from COVID-19 patients define multiple targets of vulnerability. Science.

Cao, Y., Su, B., Guo, X., Sun, W., Deng, Y., Bao, L., Zhu, Q., Zhang, X., Zheng, Y., Geng, C., *et al.* (2020). Potent Neutralizing Antibodies against SARS-CoV-2 Identified by High-Throughput Single-Cell Sequencing of Convalescent Patients' B Cells. Cell *182*, 73-84 e16.

Chen, X., Li, R., Pan, Z., Qian, C., Yang, Y., You, R., Zhao, J., Liu, P., Gao, L., Li, Z., *et al.* (2020). Human monoclonal antibodies block the binding of SARS-CoV-2 spike protein to angiotensin converting enzyme 2 receptor. Cell Mol Immunol *17*, 647-649.

Cheung, C.Y., Poon, L.L., Ng, I.H., Luk, W., Sia, S.F., Wu, M.H., Chan, K.H., Yuen, K.Y., Gordon, S., Guan, Y., *et al.* (2005). Cytokine responses in severe acute respiratory syndrome coronavirus-infected macrophages in vitro: possible relevance to pathogenesis. J Virol *79*, 7819-7826.

Chi, X., Yan, R., Zhang, J., Zhang, G., Zhang, Y., Hao, M., Zhang, Z., Fan, P., Dong, Y., Yang, Y., *et al.* (2020). A potent neutralizing human antibody reveals the N-terminal domain of the Spike protein of SARS-CoV-2 as a site of vulnerability.

Corbett, K.S., Edwards, D.K., Leist, S.R., Abiona, O.M., Boyoglu-Barnum, S., Gillespie, R.A., Himansu, S., Schafer, A., Ziwawo, C.T., DiPiazza, A.T., *et al.* (2020a). SARS-CoV-2 mRNA vaccine design enabled by prototype pathogen preparedness. Nature *586*, 567-571.

Corbett, K.S., Flynn, B., Foulds, K.E., Francica, J.R., Boyoglu-Barnum, S., Werner, A.P., Flach, B., O'Connell, S., Bock, K.W., Minai, M., *et al.* (2020b). Evaluation of the mRNA-1273 Vaccine against SARS-CoV-2 in Nonhuman Primates. N Engl J Med *383*, 1544-1555.

Corti, D., and Lanzavecchia, A. (2013). Broadly neutralizing antiviral antibodies. Annu Rev Immunol *31*, 705-742.

Dashti, A., DeVico, A.L., Lewis, G.K., and Sajadi, M.M. (2019). Broadly Neutralizing Antibodies against HIV: Back to Blood. Trends Mol Med *25*, 228-240.

Dekkers, G., Bentlage, A.E.H., Stegmann, T.C., Howie, H.L., Lissenberg-Thunnissen, S., Zimring, J., Rispens, T., and Vidarsson, G. (2017). Affinity of human IgG subclasses to mouse Fc gamma receptors. MAbs *9*, 767-773.

Dingens, A.S., Acharya, P., Haddox, H.K., Rawi, R., Xu, K., Chuang, G.Y., Wei, H., Zhang, B., Mascola, J.R., Carragher, B., *et al.* (2018). Complete functional mapping of infection- and vaccine-elicited antibodies against the fusion peptide of HIV. PLoS Pathog *14*, e1007159.

Dinnon, K.H., 3rd, Leist, S.R., Schafer, A., Edwards, C.E., Martinez, D.R., Montgomery, S.A., West, A., Yount, B.L., Jr., Hou, Y.J., Adams, L.E., *et al.* (2020a). A mouse-adapted model of SARS-CoV-2 to test COVID-19 countermeasures. Nature.

Dinnon, K.H., 3rd, Leist, S.R., Schafer, A., Edwards, C.E., Martinez, D.R., Montgomery, S.A., West, A., Yount, B.L., Jr., Hou, Y.J., Adams, L.E., *et al.* (2020b). A mouse-adapted model of SARS-CoV-2 to test COVID-19 countermeasures. Nature *586*, 560-566.

Du, L., and Jiang, S. (2010). Immunotherapy of SARS based on combinations of neutralizing human monoclonal antibodies. Future Virol *5*, 141-144.

FDA.gov (2020). Vaccines and Related Biological Products Advisory Committee (https://www.fda.gov/advisory-committees/advisory-committee-calendar/vaccines-and-related-biological-products-advisory-committee-december-17-2020-meeting-announcement#event-materials).

Folegatti, P.M., Ewer, K.J., Aley, P.K., Angus, B., Becker, S., Belij-Rammerstorfer, S., Bellamy, D., Bibi, S., Bittaye, M., Clutterbuck, E.A., *et al.* (2020). Safety and immunogenicity of the ChAdOx1 nCoV-19 vaccine against SARS-CoV-2: a preliminary report of a phase 1/2, single-blind, randomised controlled trial. Lancet *396*, 467-478.

Garcia-Beltran, W.F., Lam, E.C., Astudillo, M.G., Yang, D., Miller, T.E., Feldman, J., Hauser, B.M., Caradonna, T.M., Clayton, K.L., Nitido, A.D., *et al.* (2020). COVID-19 neutralizing antibodies predict disease severity and survival. medRxiv.

Graham, B.S. (2020). Rapid COVID-19 vaccine development. Science *368*, 945-946.

Group, A.-T.L.-C.S. (2020). A Neutralizing Monoclonal Antibody for Hospitalized Patients with Covid-19. New England Journal of Medicine.

Gu, J., Gong, E., Zhang, B., Zheng, J., Gao, Z., Zhong, Y., Zou, W., Zhan, J., Wang, S., Xie, Z., *et al.* (2005). Multiple organ infection and the pathogenesis of SARS. J Exp Med *202*, 415-424.

Halstead, S.B., and Katzelnick, L. (2020). COVID-19 Vaccines: Should We Fear ADE? J Infect Dis *222*, 1946-1950.

Hansen, J., Baum, A., Pascal, K.E., Russo, V., Giordano, S., Wloga, E., Fulton, B.O., Yan, Y., Koon, K., Patel, K., *et al.* (2020). Studies in humanized mice and convalescent humans yield a SARS-CoV-2 antibody cocktail. Science *369*, 1010-1014.

Hassan, A.O., Case, J.B., Winkler, E.S., Thackray, L.B., Kafai, N.M., Bailey, A.L., McCune, B.T., Fox, J.M., Chen, R.E., Alsoussi, W.B., *et al.* (2020). A SARS-CoV-2 Infection Model in Mice Demonstrates Protection by Neutralizing Antibodies. Cell *182*, 744-753 e744.

588 Haynes, B.F., Corey, L., Fernandes, P., Gilbert, P.B., Hotez, P.J., Rao, S., Santos, M.R., Schuitemaker,
589 H., Watson, M., and Arvin, A. (2020). Prospects for a safe COVID-19 vaccine. Sci Transl Med *12*.
590 Henderson, R., Edwards, R.J., Mansouri, K., Janowska, K., Stalls, V., Gobeil, S.M.C., Kopp, M., Li, D.,
591 Parks, R., Hsu, A.L., *et al.* (2020). Controlling the SARS-CoV-2 spike glycoprotein conformation. Nat
592 Struct Mol Biol *27*, 925-933.
593 Ho, M.S., Chen, W.J., Chen, H.Y., Lin, S.F., Wang, M.C., Di, J., Lu, Y.T., Liu, C.L., Chang, S.C., Chao,
594 C.L., *et al.* (2005). Neutralizing antibody response and SARS severity. Emerg Infect Dis *11*, 1730-1737.
595 Hou, Y.J., Okuda, K., Edwards, C.E., Martinez, D.R., Asakura, T., Dinnon, K.H., 3rd, Kato, T., Lee,
596 R.E., Yount, B.L., Mascenik, T.M., *et al.* (2020). SARS-CoV-2 Reverse Genetics Reveals a Variable
597 Infection Gradient in the Respiratory Tract. Cell *182*, 429-446 e414.
598 Hsieh, C.L., Goldsmith, J.A., Schaub, J.M., DiVenere, A.M., Kuo, H.C., Javanmardi, K., Le, K.C.,
599 Wrapp, D., Lee, A.G., Liu, Y., *et al.* (2020). Structure-based design of prefusion-stabilized SARS-CoV-2
600 spikes. Science *369*, 1501-1505.
601 Hui, K.P.Y., Cheung, M.C., Perera, R., Ng, K.C., Bui, C.H.T., Ho, J.C.W., Ng, M.M.T., Kuok, D.I.T.,
602 Shih, K.C., Tsao, S.W., *et al.* (2020). Tropism, replication competence, and innate immune responses of
603 the coronavirus SARS-CoV-2 in human respiratory tract and conjunctiva: an analysis in ex-vivo and in-
604 vitro cultures. Lancet Respir Med *8*, 687-695.
605 Huo, J., Le Bas, A., Ruza, R.R., Duyvesteyn, H.M.E., Mikolajek, H., Malinauskas, T., Tan, T.K., Rijal,
606 P., Dumoux, M., Ward, P.N., *et al.* (2020). Neutralizing nanobodies bind SARS-CoV-2 spike RBD and
607 block interaction with ACE2. Nat Struct Mol Biol *27*, 846-854.
608 Iwasaki, A., and Yang, Y. (2020). The potential danger of suboptimal antibody responses in COVID-19.
609 Nat Rev Immunol *20*, 339-341.
610 Jackson, L.A., Anderson, E.J., Rouphael, N.G., Roberts, P.C., Makhene, M., Coler, R.N., McCullough,
611 M.P., Chappell, J.D., Denison, M.R., Stevens, L.J., *et al.* (2020). An mRNA Vaccine against SARS-CoV-
612 2 - Preliminary Report. N Engl J Med *383*, 1920-1931.
613 Jaume, M., Yip, M.S., Cheung, C.Y., Leung, H.L., Li, P.H., Kien, F., Dutry, I., Callendret, B., Escriou,
614 N., Altmeyer, R., *et al.* (2011). Anti-severe acute respiratory syndrome coronavirus spike antibodies
615 trigger infection of human immune cells via a pH- and cysteine protease-independent FcgammaR
616 pathway. J Virol *85*, 10582-10597.
617 Jiang, S., Hillyer, C., and Du, L. (2020). Neutralizing Antibodies against SARS-CoV-2 and Other Human
618 Coronaviruses. Trends Immunol *41*, 355-359.
619 Joyner, M.J., Senefeld, J.W., Klassen, S.A., Mills, J.R., Johnson, P.W., Theel, E.S., Wiggins, C.C.,
620 Bruno, K.A., Klompas, A.M., Lesser, E.R., *et al.* (2020). Effect of Convalescent Plasma on Mortality
621 among Hospitalized Patients with COVID-19: Initial Three-Month Experience. medRxiv,
622 2020.2008.2012.20169359.
623 Ju, B., Zhang, Q., Ge, J., Wang, R., Sun, J., Ge, X., Yu, J., Shan, S., Zhou, B., Song, S., *et al.* (2020).
624 Human neutralizing antibodies elicited by SARS-CoV-2 infection. Nature *584*, 115-119.
625 Kam, Y.W., Kien, F., Roberts, A., Cheung, Y.C., Lamirande, E.W., Vogel, L., Chu, S.L., Tse, J.,
626 Guarner, J., Zaki, S.R., *et al.* (2007). Antibodies against trimeric S glycoprotein protect hamsters against
627 SARS-CoV challenge despite their capacity to mediate FcgammaRII-dependent entry into B cells in vitro.
628 Vaccine *25*, 729-740.
629 Karthik, K., Senthilkumar, T.M.A., Udhayavel, S., and Raj, G.D. (2020). Role of antibody-dependent
630 enhancement (ADE) in the virulence of SARS-CoV-2 and its mitigation strategies for the development of
631 vaccines and immunotherapies to counter COVID-19. Hum Vaccin Immunother, 1-6.
632 Lee, W.S., Wheatley, A.K., Kent, S.J., and DeKosky, B.J. (2020). Antibody-dependent enhancement and
633 SARS-CoV-2 vaccines and therapies. Nat Microbiol *5*, 1185-1191.
634 Leist, S.R., Dinnon, K.H., 3rd, Schafer, A., Tse, L.V., Okuda, K., Hou, Y.J., West, A., Edwards, C.E.,
635 Sanders, W., Fritch, E.J., *et al.* (2020a). A Mouse-Adapted SARS-CoV-2 Induces Acute Lung Injury and
636 Mortality in Standard Laboratory Mice. Cell *183*, 1070-1085 e1012.

637 Leist, S.R., Schafer, A., and Martinez, D.R. (2020b). Cell and animal models of SARS-CoV-2
638 pathogenesis and immunity. Dis Model Mech *13*.
639 Liao, H.X., Levesque, M.C., Nagel, A., Dixon, A., Zhang, R., Walter, E., Parks, R., Whitesides, J.,
640 Marshall, D.J., Hwang, K.K., *et al.* (2009). High-throughput isolation of immunoglobulin genes from
641 single human B cells and expression as monoclonal antibodies. J Virol Methods *158*, 171-179.
642 Liao, H.X., Lynch, R., Zhou, T., Gao, F., Alam, S.M., Boyd, S.D., Fire, A.Z., Roskin, K.M., Schramm,
643 C.A., Zhang, Z., *et al.* (2013). Co-evolution of a broadly neutralizing HIV-1 antibody and founder virus.
644 Nature *496*, 469-476.
645 Liu, L., Wang, P., Nair, M.S., Yu, J., Rapp, M., Wang, Q., Luo, Y., Chan, J.F., Sahi, V., Figueroa, A., *et*
646 *al.* (2020a). Potent neutralizing antibodies against multiple epitopes on SARS-CoV-2 spike. Nature *584*,
647 450-456.
648 Liu, Y., Soh, W.T., Tada, A., Arakawa, A., Matsuoka, S., Nakayama, E.E., Li, S., Ono, C., Torii, S.,
649 Kishida, K., *et al.* (2020b). An infectivity-enhancing site on the SARS-CoV-2 spike protein is targeted by
650 COVID-19 patient antibodies. bioRxiv, 2020.2012.2018.423358.
651 Menachery, V.D., Yount, B.L., Jr., Sims, A.C., Debbink, K., Agnihothram, S.S., Gralinski, L.E., Graham,
652 R.L., Scobey, T., Plante, J.A., Royal, S.R., *et al.* (2016). SARS-like WIV1-CoV poised for human
653 emergence. Proc Natl Acad Sci U S A *113*, 3048-3053.
654 Mulligan, M.J., Lyke, K.E., Kitchin, N., Absalon, J., Gurtman, A., Lockhart, S., Neuzil, K., Raabe, V.,
655 Bailey, R., Swanson, K.A., *et al.* (2020). Phase I/II study of COVID-19 RNA vaccine BNT162b1 in
656 adults. Nature *586*, 589-593.
657 Pak, J.E., Sharon, C., Satkunarajah, M., Auperin, T.C., Cameron, C.M., Kelvin, D.J., Seetharaman, J.,
658 Cochrane, A., Plummer, F.A., Berry, J.D., *et al.* (2009). Structural insights into immune recognition of
659 the severe acute respiratory syndrome coronavirus S protein receptor binding domain. J Mol Biol *388*,
660 815-823.
661 Pinto, D., Park, Y.J., Beltramello, M., Walls, A.C., Tortorici, M.A., Bianchi, S., Jaconi, S., Culap, K.,
662 Zatta, F., De Marco, A., *et al.* (2020). Cross-neutralization of SARS-CoV-2 by a human monoclonal
663 SARS-CoV antibody. Nature *583*, 290-295.
664 Polack, F.P., Thomas, S.J., Kitchin, N., Absalon, J., Gurtman, A., Lockhart, S., Perez, J.L., Perez Marc,
665 G., Moreira, E.D., Zerbini, C., *et al.* (2020). Safety and Efficacy of the BNT162b2 mRNA Covid-19
666 Vaccine. N Engl J Med.
667 Robbiani, D.F., Gaebler, C., Muecksch, F., Lorenzi, J.C.C., Wang, Z., Cho, A., Agudelo, M., Barnes,
668 C.O., Gazumyan, A., Finkin, S., *et al.* (2020). Convergent antibody responses to SARS-CoV-2 in
669 convalescent individuals. Nature *584*, 437-442.
670 Rockx, B., Kuiken, T., Herfst, S., Bestebroer, T., Lamers, M.M., Oude Munnink, B.B., de Meulder, D.,
671 van Amerongen, G., van den Brand, J., Okba, N.M.A., *et al.* (2020). Comparative pathogenesis of
672 COVID-19, MERS, and SARS in a nonhuman primate model. Science *368*, 1012-1015.
673 Rogers, T.F., Zhao, F., Huang, D., Beutler, N., Burns, A., He, W.T., Limbo, O., Smith, C., Song, G.,
674 Woehl, J., *et al.* (2020). Isolation of potent SARS-CoV-2 neutralizing antibodies and protection from
675 disease in a small animal model. Science *369*, 956-963.
676 Schafer, A., Muecksch, F., Lorenzi, J.C.C., Leist, S.R., Cipolla, M., Bournazos, S., Schmidt, F., Maison,
677 R.M., Gazumyan, A., Martinez, D.R., *et al.* (2021). Antibody potency, effector function, and
678 combinations in protection and therapy for SARS-CoV-2 infection in vivo. J Exp Med *218*.
679 Sempowski, G.D., Saunders, K.O., Acharya, P., Wiehe, K.J., and Haynes, B.F. (2020). Pandemic
680 Preparedness: Developing Vaccines and Therapeutic Antibodies For COVID-19. Cell *181*, 1458-1463.
681 Shi, R., Shan, C., Duan, X., Chen, Z., Liu, P., Song, J., Song, T., Bi, X., Han, C., Wu, L., *et al.* (2020). A
682 human neutralizing antibody targets the receptor-binding site of SARS-CoV-2. Nature *584*, 120-124.
683 Takada, A., Ebihara, H., Feldmann, H., Geisbert, T.W., and Kawaoka, Y. (2007). Epitopes required for
684 antibody-dependent enhancement of Ebola virus infection. J Infect Dis *196 Suppl 2*, S347-356.
685 Ubol, S., and Halstead, S.B. (2010). How innate immune mechanisms contribute to antibody-enhanced
686 viral infections. Clin Vaccine Immunol *17*, 1829-1835.

687 Ulrich, H., Pillat, M.M., and Tarnok, A. (2020). Dengue Fever, COVID-19 (SARS-CoV-2), and
688 Antibody-Dependent Enhancement (ADE): A Perspective. Cytometry A *97*, 662-667.
689 Walls, A.C., Park, Y.J., Tortorici, M.A., Wall, A., McGuire, A.T., and Veesler, D. (2020). Structure,
690 Function, and Antigenicity of the SARS-CoV-2 Spike Glycoprotein. Cell *181*, 281-292 e286.
691 Wan, Y., Shang, J., Sun, S., Tai, W., Chen, J., Geng, Q., He, L., Chen, Y., Wu, J., Shi, Z., *et al.* (2020).
692 Molecular Mechanism for Antibody-Dependent Enhancement of Coronavirus Entry. J Virol *94*.
693 Wang, C., Li, W., Drabek, D., Okba, N.M.A., van Haperen, R., Osterhaus, A., van Kuppeveld, F.J.M.,
694 Haagmans, B.L., Grosveld, F., and Bosch, B.J. (2020a). A human monoclonal antibody blocking SARS-
695 CoV-2 infection. Nat Commun *11*, 2251.
696 Wang, Q., Zhang, L., Kuwahara, K., Li, L., Liu, Z., Li, T., Zhu, H., Liu, J., Xu, Y., Xie, J., *et al.* (2016).
697 Immunodominant SARS Coronavirus Epitopes in Humans Elicited both Enhancing and Neutralizing
698 Effects on Infection in Non-human Primates. ACS Infect Dis *2*, 361-376.
699 Wang, Q., Zhang, Y., Wu, L., Niu, S., Song, C., Zhang, Z., Lu, G., Qiao, C., Hu, Y., Yuen, K.Y., *et al.*
700 (2020b). Structural and Functional Basis of SARS-CoV-2 Entry by Using Human ACE2. Cell *181*, 894-
701 904 e899.
702 Wang, S.F., Tseng, S.P., Yen, C.H., Yang, J.Y., Tsao, C.H., Shen, C.W., Chen, K.H., Liu, F.T., Liu,
703 W.T., Chen, Y.M., *et al.* (2014). Antibody-dependent SARS coronavirus infection is mediated by
704 antibodies against spike proteins. Biochem Biophys Res Commun *451*, 208-214.
705 Wec, A.Z., Wrapp, D., Herbert, A.S., Maurer, D.P., Haslwanter, D., Sakharkar, M., Jangra, R.K.,
706 Dieterle, M.E., Lilov, A., Huang, D., *et al.* (2020). Broad neutralization of SARS-related viruses by
707 human monoclonal antibodies. Science *369*, 731-736.
708 Wrapp, D., De Vlieger, D., Corbett, K.S., Torres, G.M., Wang, N., Van Breedam, W., Roose, K., van
709 Schie, L., Team, V.-C.C.-R., Hoffmann, M., *et al.* (2020a). Structural Basis for Potent Neutralization of
710 Betacoronaviruses by Single-Domain Camelid Antibodies. Cell *181*, 1004-1015 e1015.
711 Wrapp, D., Wang, N., Corbett, K.S., Goldsmith, J.A., Hsieh, C.L., Abiona, O., Graham, B.S., and
712 McLellan, J.S. (2020b). Cryo-EM structure of the 2019-nCoV spike in the prefusion conformation.
713 Science *367*, 1260-1263.
714 Wu, F., Yan, R., Liu, M., Liu, Z., Wang, Y., Luan, D., Wu, K., Song, Z., Sun, T., Ma, Y., *et al.* (2020a).
715 Antibody-dependent enhancement (ADE) of SARS-CoV-2 infection in recovered COVID-19 patients:
716 studies based on cellular and structural biology analysis. medRxiv, 2020.2010.2008.20209114.
717 Wu, Y., Wang, F., Shen, C., Peng, W., Li, D., Zhao, C., Li, Z., Li, S., Bi, Y., Yang, Y., *et al.* (2020b). A
718 noncompeting pair of human neutralizing antibodies block COVID-19 virus binding to its receptor
719 ACE2. Science *368*, 1274-1278.
720 Xu, J., Jia, W., Wang, P., Zhang, S., Shi, X., Wang, X., and Zhang, L. (2019). Antibodies and vaccines
721 against Middle East respiratory syndrome coronavirus. Emerg Microbes Infect *8*, 841-856.
722 Xu, K., Acharya, P., Kong, R., Cheng, C., Chuang, G.Y., Liu, K., Louder, M.K., O'Dell, S., Rawi, R.,
723 Sastry, M., *et al.* (2018). Epitope-based vaccine design yields fusion peptide-directed antibodies that
724 neutralize diverse strains of HIV-1. Nat Med *24*, 857-867.
725 Yilla, M., Harcourt, B.H., Hickman, C.J., McGrew, M., Tamin, A., Goldsmith, C.S., Bellini, W.J., and
726 Anderson, L.J. (2005). SARS-coronavirus replication in human peripheral monocytes/macrophages.
727 Virus Res *107*, 93-101.
728 Yip, M.S., Leung, H.L., Li, P.H., Cheung, C.Y., Dutry, I., Li, D., Daeron, M., Bruzzone, R., Peiris, J.S.,
729 and Jaume, M. (2016). Antibody-dependent enhancement of SARS coronavirus infection and its role in
730 the pathogenesis of SARS. Hong Kong Med J *22*, 25-31.
731 Yip, M.S., Leung, N.H., Cheung, C.Y., Li, P.H., Lee, H.H., Daeron, M., Peiris, J.S., Bruzzone, R., and
732 Jaume, M. (2014). Antibody-dependent infection of human macrophages by severe acute respiratory
733 syndrome coronavirus. Virol J *11*, 82.
734 Zhou, D., Duyvesteyn, H.M.E., Chen, C.P., Huang, C.G., Chen, T.H., Shih, S.R., Lin, Y.C., Cheng, C.Y.,
735 Cheng, S.H., Huang, Y.C., *et al.* (2020). Structural basis for the neutralization of SARS-CoV-2 by an
736 antibody from a convalescent patient. Nat Struct Mol Biol *27*, 950-958.

737 Zhou, J., Chu, H., Li, C., Wong, B.H., Cheng, Z.S., Poon, V.K., Sun, T., Lau, C.C., Wong, K.K., Chan,
738 J.Y., *et al.* (2014). Active replication of Middle East respiratory syndrome coronavirus and aberrant
739 induction of inflammatory cytokines and chemokines in human macrophages: implications for
740 pathogenesis. J Infect Dis *209*, 1331-1342.
741 Zost, S.J., Gilchuk, P., Case, J.B., Binshtein, E., Chen, R.E., Nkolola, J.P., Schafer, A., Reidy, J.X.,
742 Trivette, A., Nargi, R.S., *et al.* (2020a). Potently neutralizing and protective human antibodies against
743 SARS-CoV-2. Nature *584*, 443-449.
744 Zost, S.J., Gilchuk, P., Chen, R.E., Case, J.B., Reidy, J.X., Trivette, A., Nargi, R.S., Sutton, R.E.,
745 Suryadevara, N., Chen, E.C., *et al.* (2020b). Rapid isolation and profiling of a diverse panel of human
746 monoclonal antibodies targeting the SARS-CoV-2 spike protein. Nat Med *26*, 1422-1427.
747

748

Figure 1

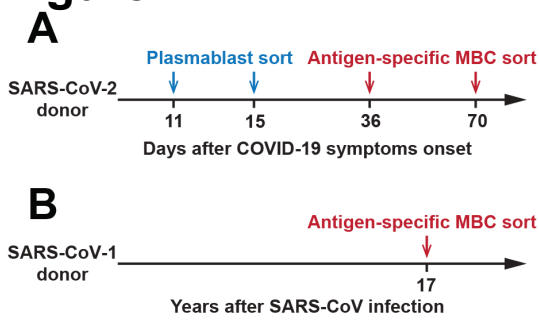

C

Donor	Cell Type	B cells sorted	SARS-CoV-2 Abs	RBD	NTD	S2	Spike only	NP
SARS-CoV-2 donor	Plasmablasts	773	101	11	4	42	1	43
SARS-CoV-2 donor	Memory B cells	594	307	121	58	99	29	NA
SARS-CoV-1 donor	Memory B cells	370	55	18	7	7	23	NA
Total		1737	463	150	69	148	53	43
Down-selected for production		NA	187	81	41	65	0	0

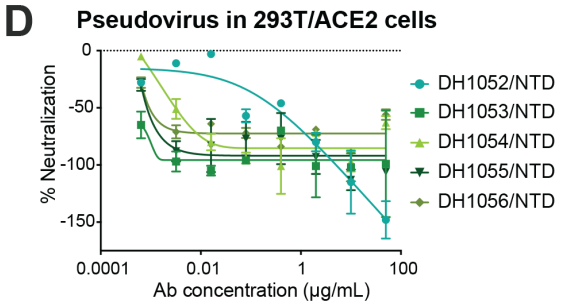

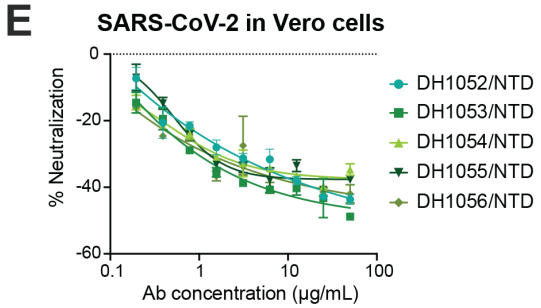

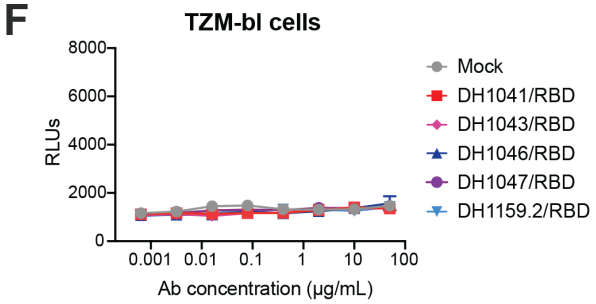

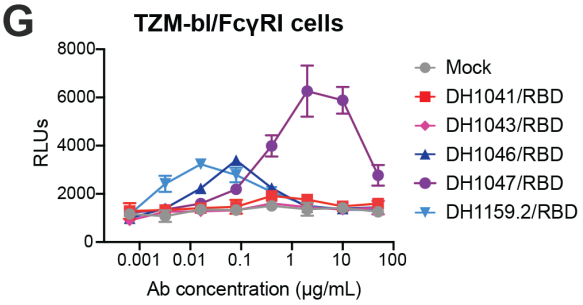

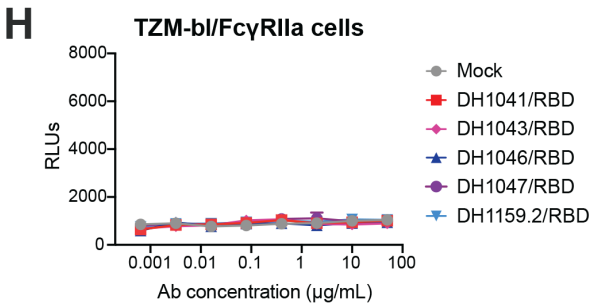

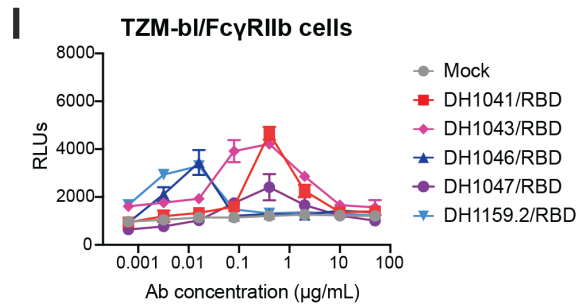

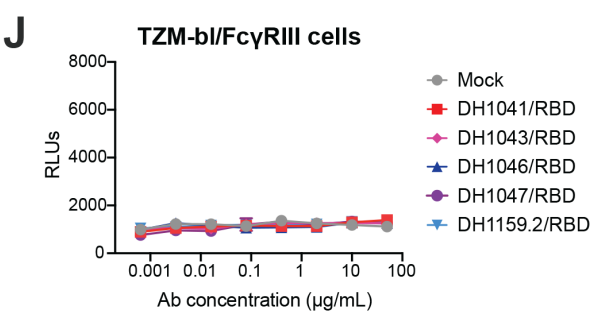

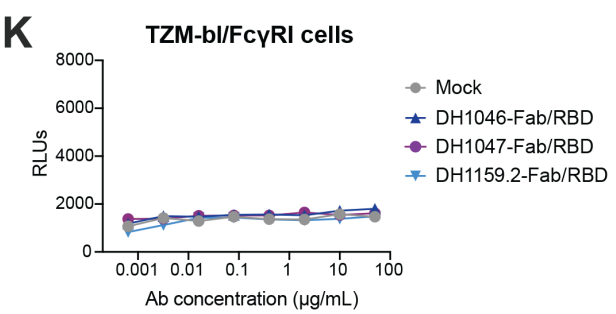

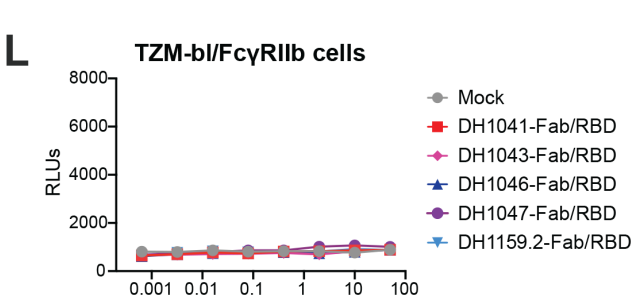

Figure 1. SARS-CoV-2 receptor-binding domain (RBD) and N-terminal domain (NTD) antibodies mediate FcγR-dependent and FcγR-independent enhancement of SARS-CoV-2 infection respectively.

(A-B) Timeline of blood sampling and antibody isolation from convalescent SARS-CoV-2 and SARS-CoV-1 donors. Plasmablasts and/or antigen-specific memory B cells (MBC) were sorted from a (A) SARS-CoV-2 infected individual (SARS-CoV-2 donor) and a (B) 2003 SARS survivor (SARS-CoV-1 donor).

(C) Summary of number and specificity of antibodies isolated from each donor.

(D-E) FcγR-independent SARS-CoV-2 infection-enhancement mediated by non-neutralizing NTD antibodies. *In vitro* neutralization curves for NTD infection-enhancing antibodies against (D) pseudotyped SARS-CoV-2 D614G in 293T-hACE2 cells, and (E) replication-competent nano-luciferase (nLuc) SARS-CoV-2 in Vero cells.

(F-J) FcγR-dependent SARS-CoV-2 infection-enhancement in ACE2-negative cells mediated by neutralizing RBD antibodies. Pseudotyped SARS-CoV-2 incubated with RBD antibodies or mock medium control were inoculated on (F) parental TZM-bl cells, and TZM-bl cells stably expressing human FcγR receptors (G) FcγRI, (H) FcγRIIa, (I) FcγRIIb or (J) FcγRIII.

(**K-L**)The effect of RBD antibody fragment antigen-binding regions (Fabs) on pseudotyped SARS-CoV-2 D614G infection were tested in (K) FcγRI-expressing TZM-bl cells and (L) FcγRIIb-expressing TZM-bl cells. Relative luminescence units (RLUs) were measured in cell lysate at 68-72 hours post-infection. Upward deflection of RLUs in the presence of antibody indicates FcγR-mediated infection. Three or four independent experiments were performed and representative data are shown.

Figure 2

A

Antibody	Epitope	Effect on SARS-CoV-2 infection: ACE2^{pos} FcγR^{neg} cells	Effect on SARS-CoV-2 infection: ACE2^{neg} FcγR^{pos} cells	Cross-reactivity with SARS-CoV-1	ACE2 blocking: IC_{50}	ACE2 blocking: IC_{80}	SARS-CoV-2 pseudovirus: IC_{50}	SARS-CoV-2 pseudovirus: IC_{80}	SARS-CoV-2 pseudovirus: Maximal% inhibition	SARS-CoV-2 replication competent virus: MN titer	SARS-CoV-2 replication competent virus: IC_{50}	SARS-CoV-2 replication competent virus: IC_{80}
DH1041	RBD				0.036	0.497	0.017	0.049	>100	0.098	0.016	0.063
DH1043	RBD				0.043	0.280	0.0015	0.020	>100	0.098	0.034	0.099
DH1159.2	RBD				>50	>50	11.900	>50	77.0	>100	ND	ND
DH1046	RBD				0.201	6.512	0.396	2.030	>100	12.500	1.086	9.383
DH1047	RBD				0.078	0.567	0.090	0.360	>100	1.100	0.124	0.666
DH1042	RBD				0.059	0.371	0.011	0.053	>100	0.280	0.071	0.269
DH1044	RBD				>50	>50	0.021	0.080	98.0	0.550	0.076	0.273
DH1045	RBD				0.226	24.353	0.380	2.260	>100	6.250	1.437	4.827
DH1052	NTD				>50	>50	>50	>50	-148.0	>100	>100	>100
DH1053	NTD				>50	>50	>50	>50	-99.0	>100	>100	>100
DH1054	NTD				>50	>50	>50	>50	-63.0	>100	>100	>100
DH1055	NTD				>50	>50	>50	>50	-106.0	>100	>100	>100
DH1056	NTD				>50	>50	>50	>50	-56.0	>100	>100	>100
DH1048	NTD				>50	>50	0.520	>50	72.0	0.390	0.608	2.232
DH1049	NTD				>50	>50	>50	>50	49.0	0.390	0.385	3.539
DH1050.2	NTD				>50	>50	0.280	>50	67.0	0.780	0.087	1.187
DH1051	NTD				>50	>50	0.049	>50	68.0	0.780	0.134	0.737
DH1050.1	NTD				>50	>50	0.039	>50	62.0	0.780	0.161	0.614

Effect on SARS-CoV-2 infection
- No effect
- Infection-enhancing
- Neutralizing

Cross-reactivity
- Non-reactive
- Reactive

Neutralization titer or blocking titer (μg/mL)
- <0.01
- 0.01-0.1
- 0.1-1
- 1-10
- 10-50
- >50

B

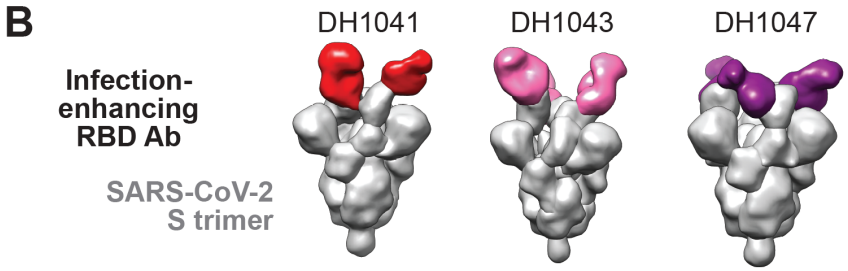

C

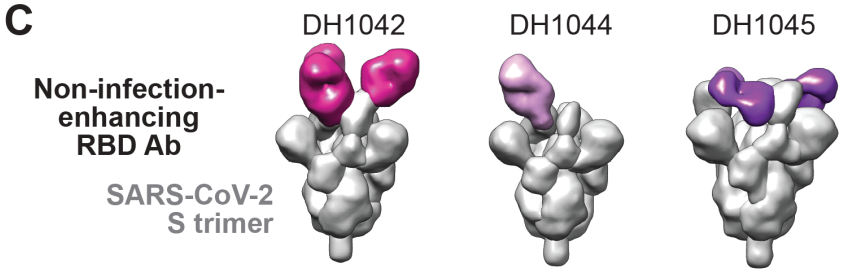

D

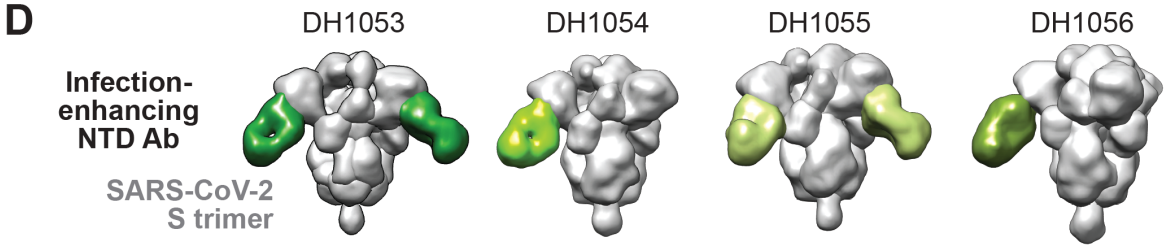

E

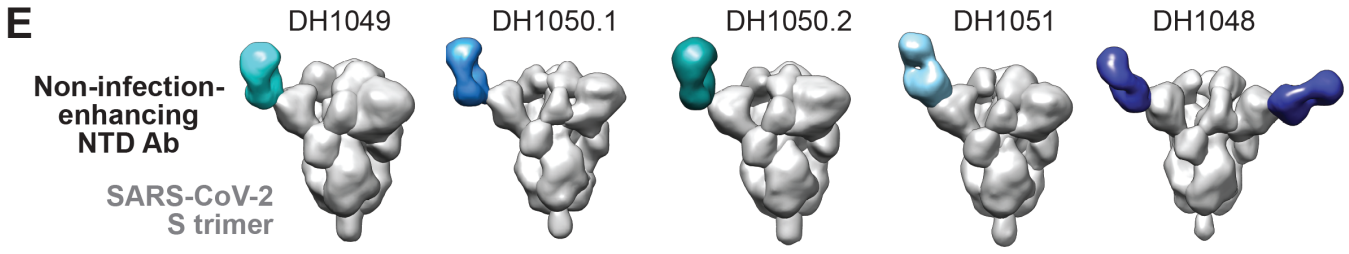

Figure 2. Structural and phenotypic characterization of infection-enhancing and non-infection-enhancing RBD and NTD antibodies.
(A) Phenotypic summary of antibodies selected for in-depth characterization. Antibody functions are color-coded based on the key shown at the right. The heatmap denotes for each antibody the epitope location, neutralizing or infection-enhancing activity in ACE2-positive/FcγR-negative cells or ACE2-negative/FcγR-positive cells. Additionally, the heatmap indicates the ability of each antibody to bind to SARS-CoV-1 S protein by ELISA, the ability of each antibody to block ACE2 binding to SARS-CoV-2 S protein, and neutralization titers against SARS-CoV-2 pseudovirus and replication-competent virus. MN titer, micro-neutralization titer; ND, not determined.
(B-E) 3D reconstruction of negative stain electron microscopy images of SARS-CoV-2 Spike ectodomain trimers stabilized with 2 proline mutations (S-2P; gray) bound to (B) infection-enhancing RBD antibody Fabs, (C) non-infection-enhancing RBD antibody Fabs, (D) infection-enhancing NTD antibody Fabs, (E) non-infection-enhancing NTD antibody Fabs. Fabs are pseudo-colored according to the phenotypic category to which they belong.

Figure 3

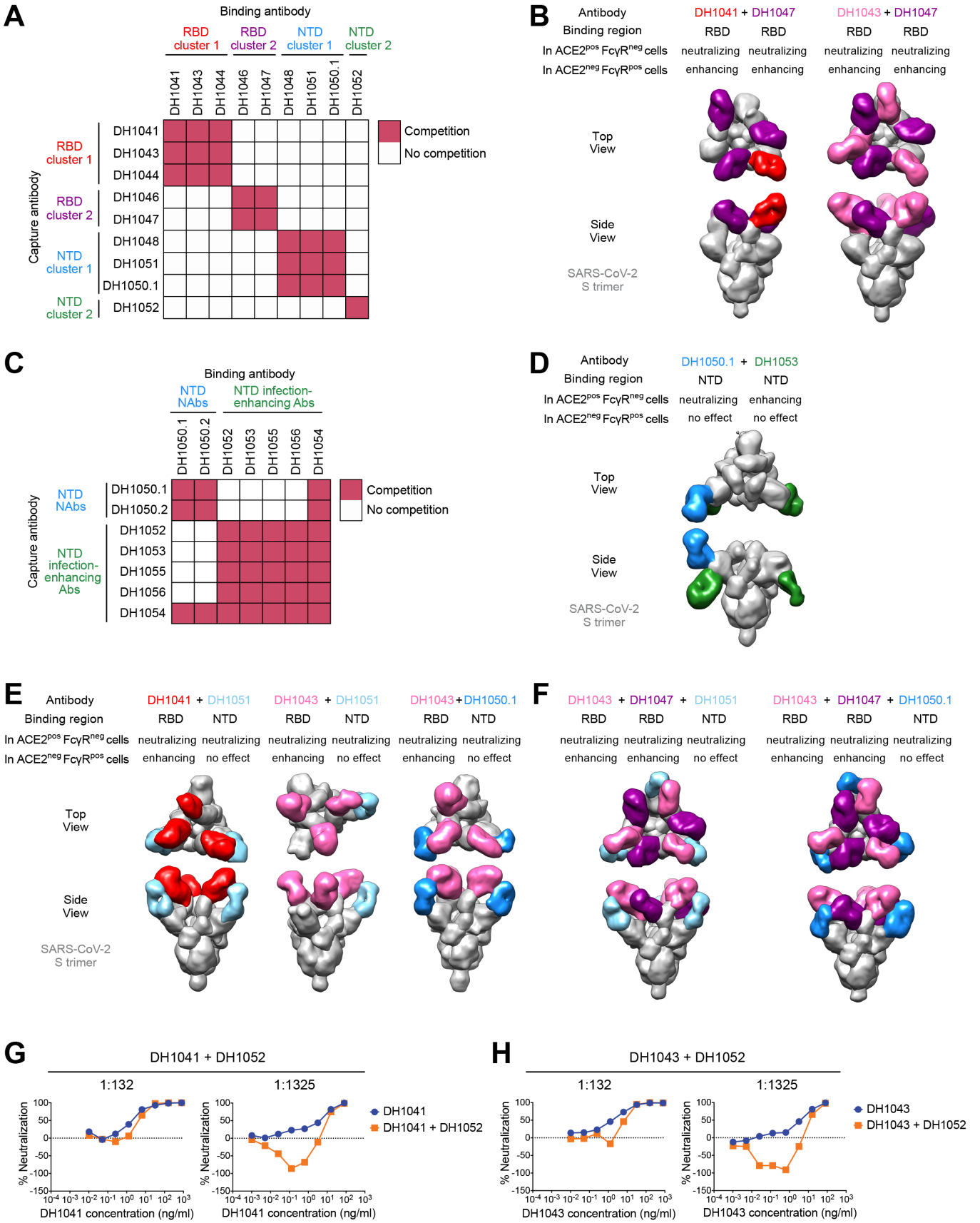
A
Binding antibody
RBD cluster 1
RBD cluster 2
NTD cluster 1
NTD cluster 2
DH1041
DH1043
DH1044
DH1046
DH1047
DH1048
DH1051
DH1050.1
DH1052
Capture antibody
Competition
No competition
B
Antibody
Binding region
In ACE2pos FcγRneg cells
In ACE2neg FcγRpos cells
DH1041 + DH1047
DH1043 + DH1047
RBD
neutralizing
enhancing
Top View
Side View
SARS-CoV-2 S trimer
C
Binding antibody
NTD NAbs
NTD infection-enhancing Abs
DH1050.1
DH1050.2
DH1052
DH1053
DH1055
DH1056
DH1054
Capture antibody
Competition
No competition
D
Antibody
Binding region
In ACE2pos FcγRneg cells
In ACE2neg FcγRpos cells
DH1050.1 + DH1053
NTD
neutralizing
enhancing
no effect
Top View
Side View
SARS-CoV-2 S trimer
E
Antibody
Binding region
In ACE2pos FcγRneg cells
In ACE2neg FcγRpos cells
DH1041 + DH1051
DH1043 + DH1051
DH1043 + DH1050.1
RBD
NTD
neutralizing
enhancing
no effect
Top View
Side View
SARS-CoV-2 S trimer
F
DH1043 + DH1047 + DH1051
DH1043 + DH1047 + DH1050.1
RBD
RBD
NTD
neutralizing
enhancing
no effect
G
DH1041 + DH1052
1:132
1:1325
% Neutralization
DH1041 concentration (ng/ml)
DH1041
DH1041 + DH1052
H
DH1043 + DH1052
1:132
1:1325
% Neutralization
DH1043 concentration (ng/ml)
DH1043
DH1043 + DH1052

Figure 3. Biophysical and structural determination that infection-enhancing and non-infection enhancing antibodies can simultaneously bind to the same S protein.
(A) Cross-blocking activity of RBD and NTD neutralizing antibodies tested by surface plasmon resonance (SPR). Soluble, stabilized SARS-CoV-2 S trimer (S-2P) was captured by the antibody on the Y-axis followed by binding by the antibody on the X-axis. Antibody binding was considered competitive (red squares) if the binding antibody did not react with the captured S protein.
(B) 3D reconstruction of simultaneous recognition of SARS-CoV-2 S-2P trimer by two RBD antibodies DH1041+DH1047, or DH1043+DH1047. All three antibodies are SARS-CoV-2 infection-enhancing in ACE2-negative/FcγR-positive cells, but neutralizing in ACE2-positive/FcγR-negative cells.
(C) Cross-blocking activity of neutralizing antibodies and infection-enhancing NTD antibodies tested by SPR. SARS-CoV-2 S-2P trimer was captured by the antibody on the Y-axis followed by binding by the antibody on the X-axis. Antibody binding was considered competitive (red squares) if the binding antibody did not react with the captured S protein.
(D) 3D reconstruction of by NTD antibodies DH1053 and DH1050.1 simultaneously bound to SARS-CoV-2 S trimer protein. In ACE2-positive/FcγR-negative cells, DH1050.1 is neutralizing while DH1053 enhances SARS-CoV-2 infection. Both antibodies have no effect in ACE2-negative/FcγR-positive cells.
(E) 3D reconstruction of SARS-CoV-2 S protein simultaneously bound to a RBD infection-enhancing antibody and a NTD non-infection-enhancing antibody. All of these antibodies neutralize SARS-CoV-2 infection of ACE2-positive/FcγR-negative cells.
(F) 3D reconstruction of SARS-CoV-2 S protein bound to triple-antibody combinations of RBD antibody DH1043, RBD antibody DH1047, and either NTD antibody DH1051 (left) or DH1050.1 (right). Both RBD antibodies enhance SARS-CoV-2 infection of ACE2-negative/FcγR-positive cells, but neutralize infection of ACE2-positive/FcγR-negative cells. NTD antibodies DH1051 and DH1050.1 neutralize SARS-CoV-2 infection of ACE2-negative/FcγR-positive cells, but have no effect on infection of ACE2-negative/FcγR-positive cells.
(G-H) RBD antibody neutralization of SARS-CoV-2 pseudovirus infection of ACE2-expressing cells in the presence of infection-enhancing NTD antibody DH1052. The infection-enhancing NTD antibody DH1052 was mixed with RBD antibodies DH1041 **(G)** or DH1043 **(H)** in 1:132 ratio or 1:1,325 ratio, respectively. Serial dilutions of the NTD:RBD antibody mixtures (orange), as well as RBD antibody alone (blue) were examined for neutralization of SARS-CoV-2 D614G pseudovirus infection of 293T/ACE2 cells.

Figure 4

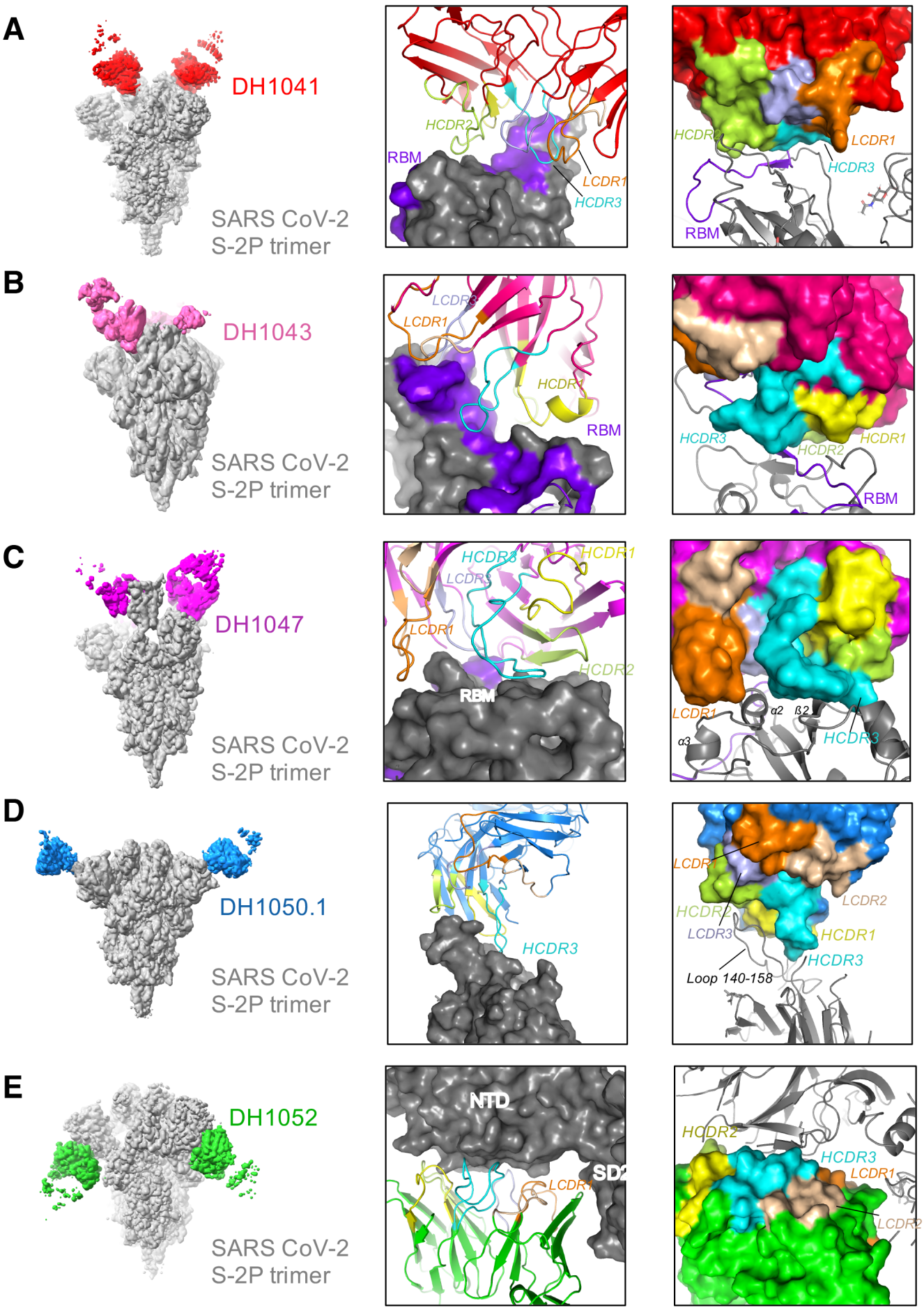
A
DH1041
SARS CoV-2
S-2P trimer
HCDR2
RBM
LCDR1
HCDR3
HCDR2
LCDR1
HCDR3
RBM
B
DH1043
SARS CoV-2
S-2P trimer
LCDR3
LCDR1
HCDR1
RBM
HCDR3
HCDR2
HCDR1
RBM
C
DH1047
SARS CoV-2
S-2P trimer
HCDR3
HCDR1
LCDR3
LCDR1
HCDR2
RBM
LCDR1
α2
ß2
α3
HCDR3
D
DH1050.1
SARS CoV-2
S-2P trimer
HCDR3
LCDR1
LCDR2
HCDR2
LCDR3
HCDR1
HCDR3
Loop 140-158
E
DH1052
SARS CoV-2
S-2P trimer
NTD
SD2
LCDR1
HCDR2
HCDR3
LCDR1
LCDR2

Figure 4. Cryo-electron microscopy of neutralizing and non-neutralizing antibodies in complex with SARS-CoV-2 Spike ectodomain. Structures of SARS-CoV-2 S protein in complex with RBD antibodies (**A)** DH1041 (red), (**B)** DH1043 (pink), (**C)** DH1047 (magenta), (**D)** neutralizing NTD antibody DH1050.1 (blue), and (**E)** infection-enhancing NTD antibody DH1052 (green). Each antibody is bound to Spike ectodomain stabilized with 2 proline mutations (S-2P) shown in gray with its Receptor Binding Motif (RBM) colored purple blue. (Right) Zoomed-in views of the antibody interactions with S-2P trimers. The antibody complementarity determining (CDR) loops are colored: HCDR1 yellow, HCDR2 limon, HCDR3 cyan, LCDR1 orange, LCDR2 wheat and LCDR3 light blue.

Figure 5

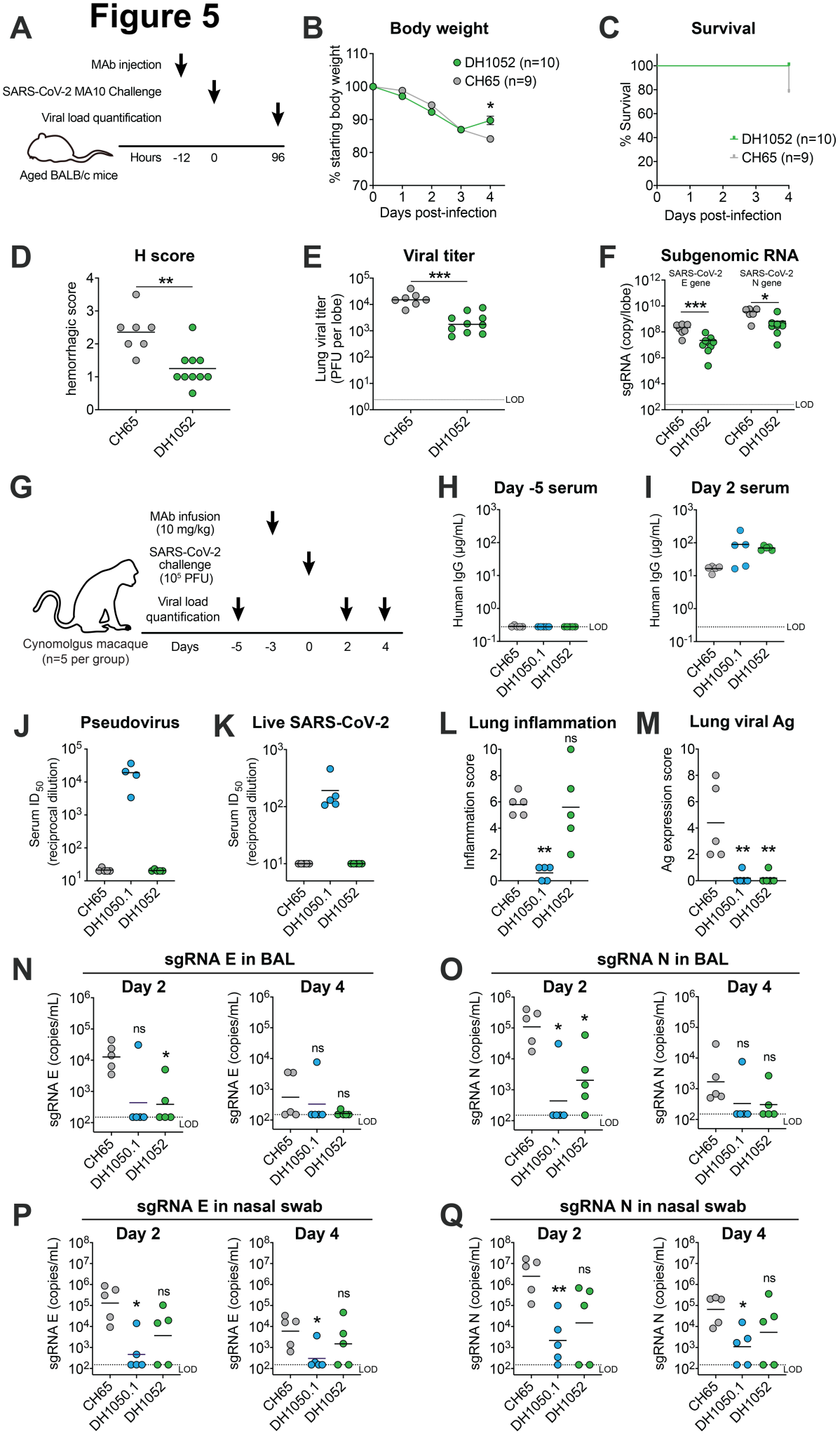
A
MAb injection
SARS-CoV-2 MA10 Challenge
Viral load quantification
Hours -12 0 96
Aged BALB/c mice
B
Body weight
% starting body weight
DH1052 (n=10)
CH65 (n=9)
Days post-infection
C
Survival
% Survival
DH1052 (n=10)
CH65 (n=9)
Days post-infection
D
H score
hemorrhagic score
CH65
DH1052
E
Viral titer
Lung viral titer (PFU per lobe)
LOD
F
Subgenomic RNA
SARS-CoV-2 E gene
SARS-CoV-2 N gene
sgRNA (copy/lobe)
G
MAb infusion (10 mg/kg)
SARS-CoV-2 challenge (10^5 PFU)
Viral load quantification
Cynomolgus macaque (n=5 per group)
Days -5 -3 0 2 4
H
Day -5 serum
Human IgG (μg/mL)
I
Day 2 serum
J
Pseudovirus
Serum ID50 (reciprocal dilution)
K
Live SARS-CoV-2
L
Lung inflammation
Inflammation score
M
Lung viral Ag
Ag expression score
CH65
DH1050.1
DH1052
N
sgRNA E in BAL
Day 2
Day 4
sgRNA E (copies/mL)
O
sgRNA N in BAL
sgRNA N (copies/mL)
P
sgRNA E in nasal swab
Q
sgRNA N in nasal swab

Figure 5. NTD antibody DH1052 enhances SARS-CoV-2 infection *in vitro*, but does not always enhance SARS-CoV-2 replication or disease *in vivo*.
(A-F) DH1052 passive immunization and murine SARS-CoV-2 challenge study design and outcome. (**A**) Diagram of the study design showing 52 week old female BALB/c mice were i.p. injected with DH1052 (200 µg/mouse, n=10, green symbols) or CH65 control antibody (gray, 200 µg/mouse, n=9, gray symbols). After 12 hours, mice were challenged with 1X10^4 PFU of mouse-adapted SARS-CoV-2 MA10 virus. Mice were euthanized and tissues were harvested 96 hours post-infection. (**B**) Body weight and (**C**) survival were monitored daily. (**D**) Hemorrhagic scores, (**E**) lung viral titers, as well as (**F**) viral subgenomic RNA (sgRNA) for both SARS-CoV-2 envelope (E) and nucleocapsid (N) gene were measured 96 hours post-infection.
(G-Q) Reduction of SARS-CoV-2 replication and disease in cynomolgus macaques by prophylactic administration of an NTD neutralizing antibody DH1050.1 or an in vitro infection-enhancing NTD Ab DH1052.
(G) Diagram of the macaque study design showing cynomolgus macaques (n=5 per group) were infused with DH1052, DH1050.1 or an irrelevant control CH65 antibody 3 days before 10^5 PFU of SARS-CoV-2 challenge via intranasal and intratracheal routes. Viral load including viral RNA and subgenomic RNA (sgRNA) were measured at the indicated pre-challenge and post-challenge timepoints. Lungs were harvested on Day 4 post-challenge for histopathology analysis.
(H-I) Serum human IgG concentrations at (**H**) Day -5 and (**I**) Day 2.
(J-K) Day 2 serum neutralization titers shown as the reciprocal serum dilution that inhibits 50% (ID_{50}) of (**J**) pseudotyped SARS-CoV-2 replication in 293T/ACE2 cells or (**K**) SARS-CoV-2 replication in Vero cells.
(L-M) Lung histopathology. Sections of the left caudal (Lc), right middle (Rm), and right caudal (Rc) lung were evaluated and scored for the presence of (**L**) inflammation by hematoxylin and eosin (H&E) staining, and for the presence of (**M**) SARS-CoV-2 nucleocapsid by immunohistochemistry (IHC) staining. Symbols indicate the sums of Lc, Rm, and Rc scores in each animal.
(N-O) SARS-CoV-2 (**N**) E gene sgRNA and (**O**) N gene sgRNA in bronchoalveolar lavage (BAL) on Day 2 and Day 4 post challenge.
(P-Q) SARS-CoV-2 (**P**) E gene sgRNA and (**Q**) N gene sgRNA in nasal swab on Day 2 and Day 4 post challenge.
LOD, limit of detection. Statistical significance in all the panels were determined using Wilcoxon rank sum exact test. Asterisks show the statistical significance between indicated group and CH65 control group: ns, not significant, *P<0.05, **P<0.001, ***P<0.0001.

Figure 6

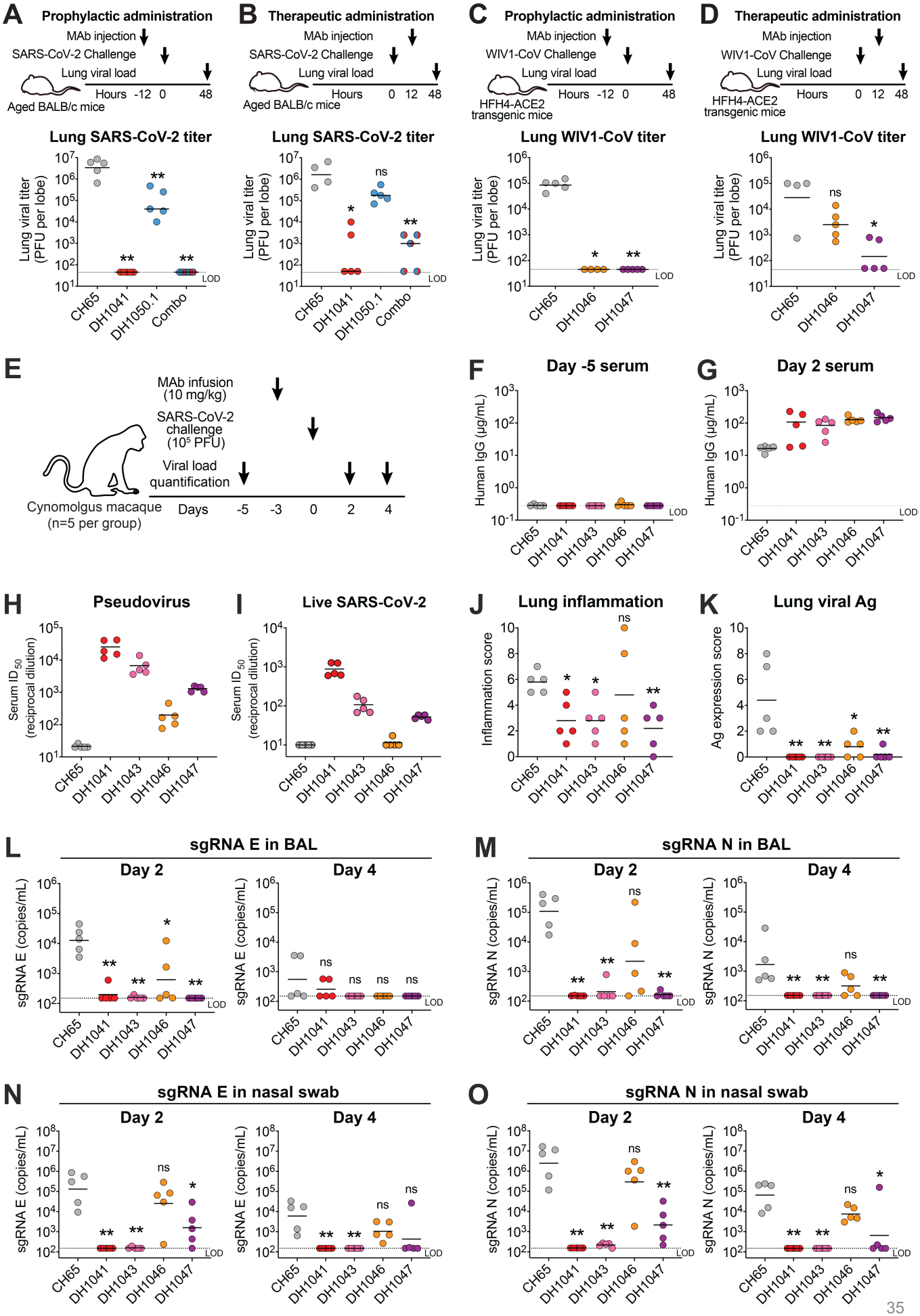
A
Prophylactic administration
MAb injection
SARS-CoV-2 Challenge
Lung viral load
Hours -12 0 48
Aged BALB/c mice
Lung SARS-CoV-2 titer
Lung viral titer (PFU per lobe)
LOD
CH65
DH1041
DH1050.1
Combo
B
Therapeutic administration
MAb injection
SARS-CoV-2 Challenge
Lung viral load
Hours 0 12 48
Aged BALB/c mice
Lung SARS-CoV-2 titer
ns
C
Prophylactic administration
MAb injection
WIV1-CoV Challenge
Lung viral load
Hours -12 0 48
HFH4-ACE2 transgenic mice
Lung WIV1-CoV titer
DH1046
DH1047
D
Therapeutic administration
MAb injection
WIV1-CoV Challenge
Lung viral load
Hours 0 12 48
HFH4-ACE2 transgenic mice
Lung WIV1-CoV titer
E
MAb infusion (10 mg/kg)
SARS-CoV-2 challenge (10^5 PFU)
Viral load quantification
Cynomolgus macaque (n=5 per group)
Days -5 -3 0 2 4
F
Day -5 serum
Human IgG (µg/mL)
DH1043
G
Day 2 serum
H
Pseudovirus
Serum ID_{50} (reciprocal dilution)
I
Live SARS-CoV-2
J
Lung inflammation
Inflammation score
K
Lung viral Ag
Ag expression score
L
sgRNA E in BAL
Day 2
Day 4
sgRNA E (copies/mL)
M
sgRNA N in BAL
sgRNA N (copies/mL)
N
sgRNA E in nasal swab
O
sgRNA N in nasal swab

Figure 6. RBD antibodies that mediate FcγR-dependent infection enhancement *in vitro*, protect mice and non-human primates from SARS-CoV-2 challenge.
(A-B) Protection in BALB/c mice against mouse-adapted SARS-CoV-2. Mice (n=5 per group) were intraperitoneally (i.p.) injected with 300 μg of a single antibody or 150 μg of two antibodies in combination (A) prophylactically at 12h pre-infection or (B) therapeutically at 12h post-infection. Infection was performed with mouse-adapted SARS-CoV-2 2AA MA virus via intranasal (i.n.) route. Titers of infectious virus in the lung were examined 48 post-infection. An irrelevant human antibody CH65 was used as a negative control.
(C-D) Protection in HFH4-hACE2-transgenic mice against SARS-related bat WIV1-CoV challenge. Mice (n=5 per group) were intraperitoneally (i.p.) injected with 300 μg of indicated antibody or CH65 control antibody (C) prophylactically at 12h pre-infection or (D) therapeutically at 12h post-infection. Infection was performed with WIV1-CoV via i.n. route. Lung viral titers were examined at 48 post-infection.
(E-O) RBD NAbs and infection-enhancing Abs protected SARS-CoV-2 infection in non-human primates.
(E) Study design. Cynomolgus macaques (n=5 per group) were infused with DH1041, DH1043, DH1046, DH1047 or an irrelevant CH65 antibody 3 days before 10^5 PFU of SARS-CoV-2 challenge via intranasal route and intratracheal route. Viral load including viral RNA and subgenomic RNA (sgRNA) were measured on the indicated pre-challenge and post-challenge timepoints. Lungs were harvested on Day 4 post-challenge for histopathology study.
(F-G) Serum human IgG concentrations at Day -5 (H) and Day 2 (I).
(H-I) Day 2 serum neutralization titers shown as the reciprocal serum dilution that inhibits 50% (ID_{50}) of (**H**) pseudotyped SARS-CoV-2 replication in 293T/ACE2 cells or (**J**) SARS-CoV-2 replication in Vero cells.
(J-K) Lung histopathology. Sections of the left caudal (Lc), right middle (Rm), and right caudal (Rc) lung were evaluated and scored for (**J**) the presence of inflammation by hematoxylin and eosin (H&E) staining, and (**K**) for the presence of SARS-CoV-2 nucleocapsid by immunohistochemistry (IHC) staining. Symbols indicate the sums of Lc, Rm, and Rc scores for each animal.
(L-M) SARS-CoV-2 (**L**) E gene sgRNA and (**M**) N gene sgRNA in bronchoalveolar lavage (BAL) on Day 2 and Day 4 post challenge.
(N-O) SARS-CoV-2 (**N**) E gene sgRNA and (**O**) N gene sgRNA in nasal swab on Day 2 and Day 4 post challenge.
Statistical significance in all the panels were determined using Wilcoxon rank sum exact test. Asterisks show the statistical significance between indicated group and CH65 control group: ns, not significant, *P<0.05, **P<0.001.